



The impact of the Neoglacial and other environmental changes on the raised beaches of Joinville Island, Antarctica

BRITTANY M. THEILEN ¹, ALEXANDER R. SIMMS ¹, REGINA DEWITT ², JULIE ZURBUCHEN ¹, CHRISTOPHER GARCIA ² and CAMERON GERNANT¹

¹Department of Earth Science, University of California Santa Barbara, 1006 Webb Hall, Santa Barbara, CA 93111, USA

²Department of Physics, East Carolina University, C-209 Howell Science Complex, Greenville, NC 27858, USA
asimms@geol.ucsb.edu

Abstract: In order to reconstruct past environmental conditions along the north-eastern Antarctic Peninsula, we documented changes in grain size, grain roundness, onlap as seen in ground-penetrating radar reflection profiles and ice-rafted debris on a set of 36 raised beaches developed over the last $\sim 7.7 \pm 0.9$ ka on Joinville Island. The most pronounced changes in beach character occur at ~ 2.7 – 3.0 ka. At this time, there appears to have been a reintroduction of less rounded material, the development of stratification within individual beach ridges, an introduction of seaweed and limpets to the beach deposits, a change in clast provenance (although slightly earlier than the change in cobble roundness) and a shallowing of the overall beach plain slope. Prolonged cooling associated with the Neoglacial period may have contributed to these changes, as the readvance of glaciers could have changed the provenance of the beach deposits and introduced more material, leading to the change in roundness of the beach cobbles and the overall slope of the beach plain. This study suggests that late Holocene environmental change left a measurable impact on the coastal zone of Antarctica.

Received 14 February 2023, accepted 3 September 2023

Key words: Climate, coastlines, glacial isostatic adjustment, Holocene, sea level, Weddell Sea

Introduction

The Antarctic Peninsula (AP) is one of the fastest-warming locations in the world and is experiencing rapid environmental changes (Vaughan *et al.* 2003, Ruiz-Fernandez *et al.* 2019, Turner *et al.* 2022, Siegert *et al.* 2023). Late Holocene palaeoenvironmental data are crucial for placing these observations of modern changes into context. Holocene climate events across the AP are recorded in high-resolution marine, lacustrine and ice-core records (Michalchuk *et al.* 2009, Mulvaney *et al.* 2012, Sterken *et al.* 2012, Totten *et al.* 2015, Cejka *et al.* 2020, Groff *et al.* 2023). Proxy data from these cores record past periods of warming and cooling driven by wind shifts, ocean circulation changes and El Niño-Southern Oscillation (ENSO) variability (Domack *et al.* 2001, Shevenell *et al.* 2011, Barbara *et al.* 2016, Nie *et al.* 2022). However, these proxy reconstructions only indirectly record environmental changes occurring within the coastal zone. One underutilized palaeoenvironmental proxy is the sedimentary characteristics of beach deposits (Scheffers *et al.* 2012, Lindhorst & Schutter 2014, Simkins *et al.*

2015), which along most Antarctic coastlines have been uplifted and thus preserved due to post-glacial rebound. Because these beach deposits reflect coastal environmental characteristics such as wave climate, sea-ice cover and iceberg density (Hall & Perry 2004, Simkins *et al.* 2015), changes in their characteristics may reflect environmental changes occurring within the coastal zone through the Holocene.

The purpose of this study is to characterize trends in ground-penetrating radar (GPR) profiles, gross morphology, grain size, clast roundness and ice-rafted debris (IRD) on raised beach deposits through the late Holocene on Joinville Island along the Eastern Antarctic Peninsula (EAP; Fig. 1). Changes in these proxies through time are hypothesized to reflect changes in the processes operating on beaches through the late Holocene and thus to reflect the environmental changes impacting the area. This archive also augments studies of palaeo-sea levels (e.g. Zurbuchen & Simms 2019) derived from the same raised beaches by providing ages for the older beach ridges and a background as to what other changes may be responsible for beach-ridge elevation changes.

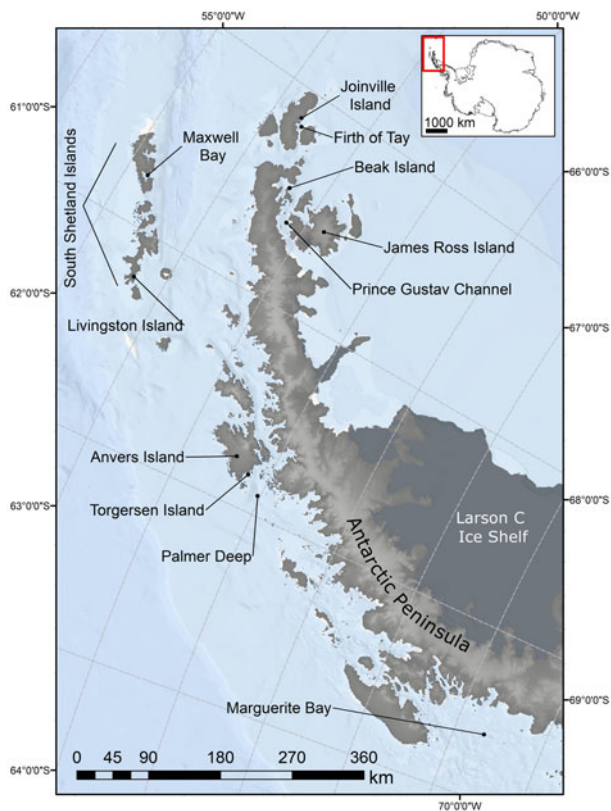


Fig. 1. Map showing the location of the field site and other places mentioned in the text.

Background

Beaches as potential archives of past environmental conditions

Wave climate provides a first-order control on beach deposit characteristics (Butler 1999). Thus, the granulometry of beach deposits may provide a proxy archive of environmental conditions impacting wave climate through time (Bentley *et al.* 2005, Simkins *et al.* 2015). The presence of sea ice restricts wave exposure and sediment supply to the beach (Nichols 1961, Butler 1999) by limiting fetch, thus decreasing wave energy. Therefore, in the absence of significant fluvial sources in the area, cooler conditions associated with sea ice and the less frequent reworking of beach cobbles are thought to be characteristic of beach deposits with more poorly rounded clasts (Nichols 1961, Butler 1999, Simkins *et al.* 2015). Warmer conditions associated with no sea ice and higher wave energy are thought to be characteristic of beach deposits consisting of more rounded clasts (Nichols 1961).

IRD prevalence is another aspect of beach deposits that provides an archive of past environmental conditions. Hall & Perry (2004) used IRD on Byers Peninsula of Livingston Island in the South Shetland Islands to create a climate proxy for the northern AP

during the Holocene. The proxy is based on IRD densities from boulder counts along beach ridges. Higher IRD counts were interpreted to represent cooler climate conditions marked by glacial advances (Hall & Perry 2004), whereas lower IRD counts were interpreted to represent warmer conditions and glacial retreat (Kanfoush *et al.* 2002).

Modern climate and oceanographic setting

The EAP is subjected to cold, saline Weddell Sea Transitional Waters from the Weddell Gyre (García *et al.* 2002) and is associated with cold continental air masses (Reynolds 1981) and extensive sea ice (Stammerjohn & Smith 1996, Domack *et al.* 2003, Ingólfsson *et al.* 2003, Michalchuk *et al.* 2009). Clockwise circulation of the Weddell Gyre brings warm Circumpolar Deep Water into the EAP (Orsi *et al.* 1993), turning the Circumpolar Deep Water into Weddell Sea Transitional Water (Barbara *et al.* 2016, Vernet *et al.* 2019). The Antarctic Sound to the west of Joinville Island is a zone of mixing between Weddell Sea waters and those from the Bransfield Basin, with waters from the Bransfield Basin being more dominant during the summer months (Krek *et al.* 2021).

Due to its extensive sea ice, the influence of southern barrier winds and fewer oceanic connections with the Pacific Ocean, the Weddell Sea sector of the AP is much cooler than other parts of the AP (Ambrozova *et al.* 2020). The coldest temperatures are recorded when winds are out of the south, whereas they are warmer when the winds blow from the north (Ambrozova *et al.* 2019). These southerly winds are sometimes referred to as 'barrier winds' and are sourced from the interior of the continent to the south of the Weddell Sea and kept on the EAP due to the presence of the mountains of the AP (Schwerdtfeger 1975). The EAP is less influenced by westerly winds, which are a key climate driver across West Antarctica (Marshall *et al.* 2006), than the western AP because the mountains located along the AP act as a barrier to winds and ocean currents (Bentley *et al.* 2009, Dickens *et al.* 2019). However, landmasses and surrounding bodies of water located at the northeastern tip of the AP might not be completely shielded or isolated from western influences due to low relief of the islands and oceanographic connections (Michalchuk *et al.* 2009, Krek *et al.* 2021).

The Weddell Sea contains the largest accumulation of multiyear sea ice in the Southern Ocean, accounting for over a third of the total sea ice in the Southern Ocean (Parkinson & Cavalleri 2012). After a steady increase in sea-ice extent through the latter half of the twentieth century, sea ice started to experience an abrupt decrease in extent after 2015, with several record low extents being noted since that time (Kumar *et al.* 2021, Parkinson & DiGirolamo 2021, Jena *et al.* 2022). Those

trends vary according to season, with a general increase occurring during summer months and a decrease occurring during winter months (Kumar *et al.* 2021). Some of these recent minimum sea-ice extents have been linked to intense storms (Jena *et al.* 2022).

Ongoing and past climate changes

Climate in the AP region behaves differently than in the continental interior of Antarctica. Although shifts in westerly winds and the Antarctic Circumpolar Current caused rapid sea-ice retreat in the western AP during the Holocene (Shevenell *et al.* 2011, Mulvaney *et al.* 2012, Barbara *et al.* 2016), Barbara *et al.* (2016) suggest that the EAP responded differently than the western AP because of the presence of the Weddell Gyre. Instead, the circulation of the gyre transported more fresh, cold surface waters and sea ice northwards, which slowed ice-shelf retreat on the EAP and delayed seasonal open water conditions. However, warming and sea-ice demise have since continued on both sides of the AP over the last 5 years (e.g. Kumar *et al.* 2021).

Over the Holocene, forcing mechanisms produced shifts in climatic conditions, including the Early Holocene Climate Optimum, the Mid-Holocene Warm Period, the Neoglacial interval, the Mediaeval Warm Period, the Little Ice Age (LIA) and the recent rapid regional warming period (Bentley *et al.* 2009). However, the various proxy records do not all record each of these climate periods. The absence of climatic events might be caused by the analysis of different proxy records. For example, a marine core taken from the Palmer Deep, Site IODP 1098, records the LIA at ~0.70–0.15 ka (Domack *et al.* 2001, Domack *et al.* 2003), whereas marine cores taken from the Firth of Tay and Maxwell Bay have no pronounced records of the LIA (Michalchuk *et al.* 2009, Milliken *et al.* 2009), even though terrestrial records nearby show clear evidence for a LIA (Kaplan *et al.* 2020, Simms *et al.* 2021).

Bentley *et al.* (2009) described each of the Holocene climate periods. The Early Holocene Climate Optimum lasted from 11.0 to 9.5 ka (Johnson *et al.* 2011). This period is characterized by significant widespread warming (Masson-Delmotte *et al.* 2004) and ice retreat across Antarctica during the early Holocene (Pudsey *et al.* 1994, Domack *et al.* 2001, Domack 2002, Evans *et al.* 2005, Bentley *et al.* 2009, Davies *et al.* 2014, Nyvlt *et al.* 2014). Deglaciation continued, most likely at a slower rate, during the period after the optimum from 9.5 to 4.5 ka, reaching a similar glacial configuration as today sometime around 5–6 ka (Johnson *et al.* 2011, Glasser *et al.* 2014, Smith *et al.* 2021), with there being some geographical variability in climatic responses (Bentley *et al.* 2009).

The Mid-Holocene Warm Period, also known as the Mid- to Late Holocene Hypsithermal, was the next

climate period of significant warming across the AP from 4.5 to 2.8 ka. This period is associated with rapid sedimentation, high organic productivity and increased species diversity in lake sediments (Björck *et al.* 1996, Hodgson *et al.* 2004, Hodgson & Convey 2005, Sterken *et al.* 2012) and reduced sea-ice coverage, greater primary production and increased marine sedimentation rates (Domack *et al.* 2003, Bentley *et al.* 2009, Totten *et al.* 2015). However, unlike the optimum, not all proxy records across the AP indicate a significant warming trend during this period, and the timing of the Mid-Holocene Warm Period varied by hundreds of years depending upon the proxy (Bentley *et al.* 2009).

A shift from warmer conditions to colder conditions marks the end of the Mid- to Late Holocene Warm Period and the start of the Neoglacial period. According to Bentley *et al.* (2009), the Neoglacial interval lasted from ~2.5 to 1.2 ka and probably started earlier on the western AP (3.6 ka; Domack 2002) than the EAP (2.5 ka; Bentley *et al.* 2009). Cejka *et al.* (2020) provide a well-documented shift to cooler conditions on the EAP from a lake record on Vega Island that suggests a slightly younger age of ~2.1 ka for the onset of the Neoglacial on the EAP. Shevenell & Kennett (2002) suggest that the earlier onset in the Palmer Deep was caused by an increase in cooler shelf waters and westerly winds. The climate conditions of this period are associated with more intense sea ice, cooler open water conditions, a decline in biological productivity and a glacial advance (Domack & McClennen 1996, Totten *et al.* 2015). Recent mapping (Carrivick *et al.* 2012), modelling (Davies *et al.* 2014) and cosmogenic dating of terrestrial moraines has constrained glacial advances to this time period as well (Kaplan *et al.* 2020, Palacios *et al.* 2020).

The Neoglacial period is in some places interrupted by the Mediaeval Warm Period, which is thought to have lasted from 1200 to 600 ka and is well documented in the Northern Hemisphere. However, evidence for a Mediaeval Warm Period in Antarctica is fragmentary, with only a few records clearly showing it, and those that do are from the western AP. This evidence includes a few marine core records (Bentley *et al.* 2009) and a period of more restricted glacial ice around Palmer Station (Hall *et al.* 2010a, Yu *et al.* 2016, Charman *et al.* 2018). Evidence for a LIA is growing across the AP. Evidence for the LIA includes glacial advances (Hall 2007, Guglielmin *et al.* 2016, Kaplan *et al.* 2020, Simms *et al.* 2021), increased sea-ice conditions and colder sea-surface temperatures (Domack *et al.* 1995, Bentley *et al.* 2009, Hall 2009, Shevenell & Kennett 2002). Recent work is beginning to suggest that the timing of the glacial advances within the AP are coeval with the LIA in the Northern Hemisphere (Hall 2009, Simms *et al.* 2021).

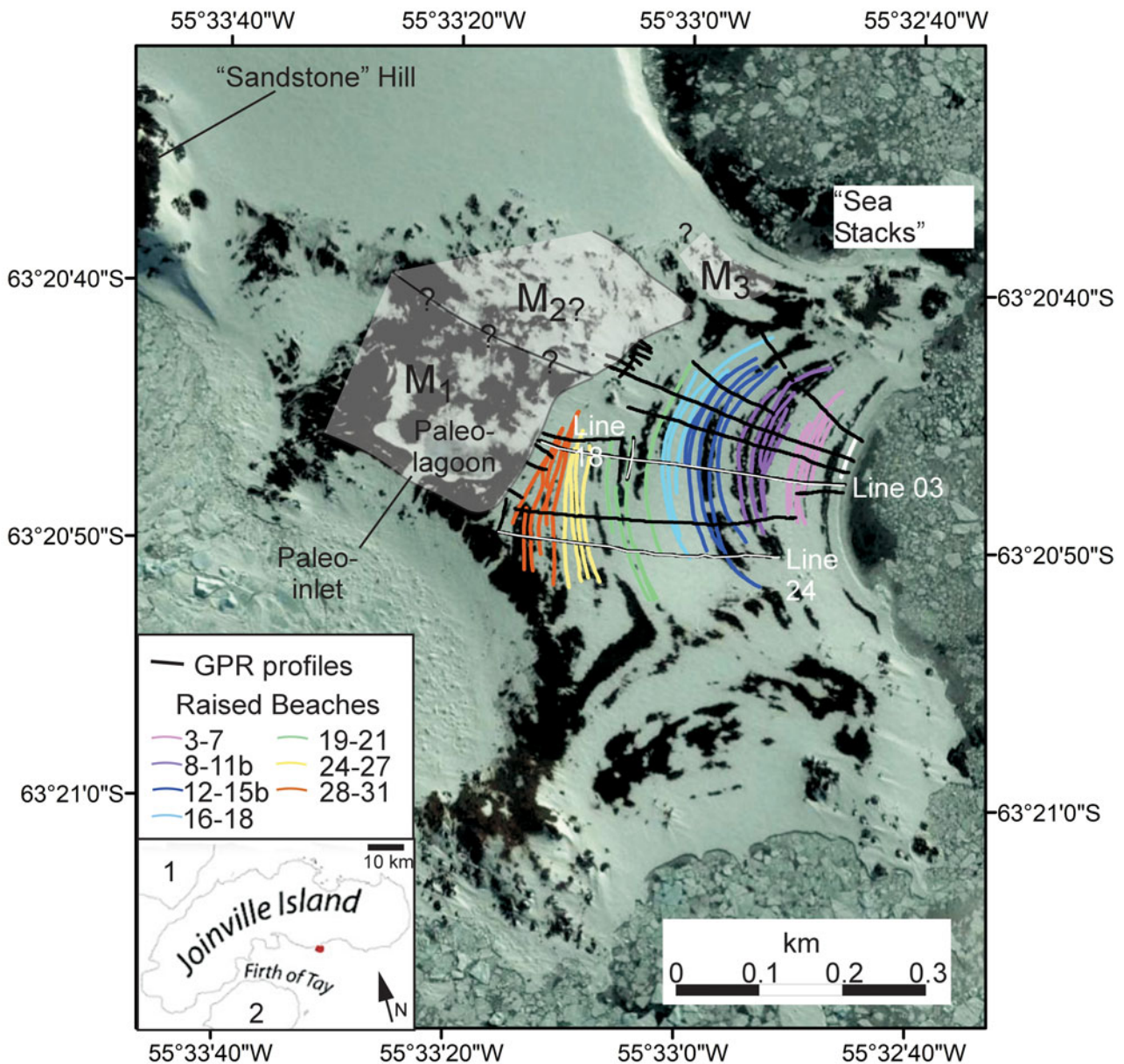


Fig. 2. Google Earth image of Tay Head on Joinville Island and the locations of the beaches, moraines (translucent grey) and ground-penetrating radar (GPR) profiles discussed in the text. Beaches 22 and 23 are not displayed because GPS data could not be processed. Inset map shows the location of Tay Head (red dot) on Joinville Island as well as the location of D'Urville Island (1) and Dundee Island (2).

The recent rapid regional warming period, following the LIA, is marked by the ongoing pronounced warming trend across Antarctica, most likely due to increased greenhouse gases in the atmosphere (Houghton 2001). The recent rapid regional warming event is associated with increased sediment accumulation rates in a variety of proxy records such as lake and marine cores (Bentley *et al.* 2009), ice retreat, paraglacial changes and reduced sea-ice durations and snow cover (Vaughan *et al.* 2003,

Ruiz-Fernandez *et al.* 2019, Turner *et al.* 2022, Siegert *et al.* 2023).

Regional sea-level reconstructions

Compared to other coastlines, relatively few studies of relative sea-level (RSL) changes are available for much of Antarctica due to limited ice-free locations. The few RSL records that do exist across the AP are found within



Fig. 3. Photographs of the field site including **a.** fabric of beach 5 deposits with well-bedded gravels and sands, **b.** fabric of beach 28 deposits lacking bedding and sands, **c.** snow cover and 1 m² 'pits' in which out-of-place pebbles were counted and **d.** sandstone outcrop on the hill.

the South Shetland Islands (Bentley *et al.* 2005, Hall 2010, Watcham *et al.* 2011, Simms *et al.* 2012), Marguerite Bay (Simkins *et al.* 2013), Torgersen Island (Simms *et al.* 2018), Alexander Island (Roberts *et al.* 2009), Beak Island (Roberts *et al.* 2011), James Ross Island (Hjort *et al.* 1997) and locally on Joinville Island (Fig. 1; Zurbuchen & Simms 2019). On Joinville Island, Zurbuchen & Simms (2019) reconstructed a record of RSL based on the topographically lower 21 of the 36 beaches on the island. Radiocarbon ages from those lower 18 beach ridges reveal that RSL has fallen 4.9 ± 0.58 m since 3.1 ka, with an abrupt, short-lived increase in the rate of RSL fall from 1.5 to 1.3 ka and a potential RSL rise from 0.7 to 0.2 ka (Zurbuchen & Simms 2019). The beaches continue to an elevation of 12.2 m, which, when corrected for the 1.3 m elevation of the modern beach ridge crest, suggests a marine limit of no less than 10.9 m, which currently remains undated.

Tay Head peninsula

Joinville Island is located at the north-eastern tip of the AP between D'Urville Island and Dundee Island (Figs 1 & 2). These islands are a geological continuation of the Trinity Peninsula (Elliot 1967). However, due to a combination of snow cover and sparse outcrops, little detailed mapping has been conducted on Joinville Island. Studies of correlative rocks on the AP itself suggest that the Trinity Peninsula consists predominantly of folded clastic Carboniferous through Cenozoic sedimentary rocks such as siltstones, sandstones and conglomerates, with their metamorphosed counterparts associated with later volcanic intrusions (Barbeau *et al.* 2010, Bradshaw *et al.* 2012, Zak *et al.* 2012).

The 36 discrete raised beach ridges (separated from one another by troughs) observed on Joinville Island are ~0.4 km long (shore parallel) and located on the east side of Tay Head, an ~2.0 km × 2.5 km peninsula positioned on the south side of Joinville Island (Fig. 2). A similar, more weakly developed series of beach ridges is found on the south-facing portions of Tay Head but were not surveyed. The field site is adjacent to the Firth of Tay, 15 km from the location of a SHALDRIL core from which Michalchuk *et al.* (2009) obtained a high-resolution record of Holocene deglacial and climate history.

Methods

Granulometry

The size and roundness of the largest 100 surface clasts within 1 m² were observed, recorded and photographed, similar to the approaches of Simkins *et al.* (2015) and Bentley *et al.* (2005). This process was repeated three times along each crest of the 36 raised beaches. Clasts

from the field and in photographs were classified into six categories: well rounded, rounded, sub-rounded, subangular, angular and very angular (Powers 1953). Grain size was measured according to the two visible axes observed in photographs. Standard deviation was used to quantify sorting.

Out-of-place pebbles

The density of out-of-place pebbles (OPPs), identified as rock types not represented in the local bedrock or till outcrops, within a 15 m³ area on the crest of each beach (Fig. 3c) was measured along every other beach to aid in the reconstruction of glacial activity and provenance. These OPPs were generally interpreted as IRD; however, we cannot conclusively rule out their original transportation by an earlier (Last Glacial Maximum?) ice sheet that covered the whole region and later reworking into the beach deposits. In addition to what appeared to be exotic OPP clasts, we also counted the number of clasts of a distinctive rhyolite found in dikes within the local bedrock and sandstone (quartzite) clasts that appeared to be sourced from a local hill to the north-west of the beaches ('Sandstone Hill'; Figs 2 & 3d). However, we are less confident in our counting of the sandstone clasts compared to the rhyolite clasts due to the similarity of the sandstone and other local finer-grained metasedimentary bedrock. The difficulty of counting was exacerbated by snow cover at the time (Fig. 3c).

GPS and tide gauge

Joinville Island GPS and tide data are reported in Zurbuchen & Simms (2019). Elevation and coordinate data were obtained using a UNAVCO Trimble Net R9 receiver global navigation satellite system (GNSS) base station and Trimble 5700 GPS/GNSS receiver. Upon failure of the local base station, the O'Higgins permanent GPS station (www.sonel.org, last accessed 10 February 2023), located ~115 km away from Joinville Island, was used instead. Beach-ridge profiles were obtained from kinematic-mode GPS surveys across the crest of each beach ridge, except for beach ridges 2 and 3, which each have three static elevation points due to the presence of wildlife. GPS data were processed in Trimble Business Center with horizontal and vertical precisions of ~0.25 m. Elevations were converted to mean sea level using 2 days of data from a locally deployed Valeport 740 Portable Water Level Recorder (tide gauge) matched to the tide gauge at Bahia Esperanza ~50 km away.

Ground-penetrating radar

Approximately 2.5 km of GPR profiles were collected across the beaches of Tay Head using a Sensors and

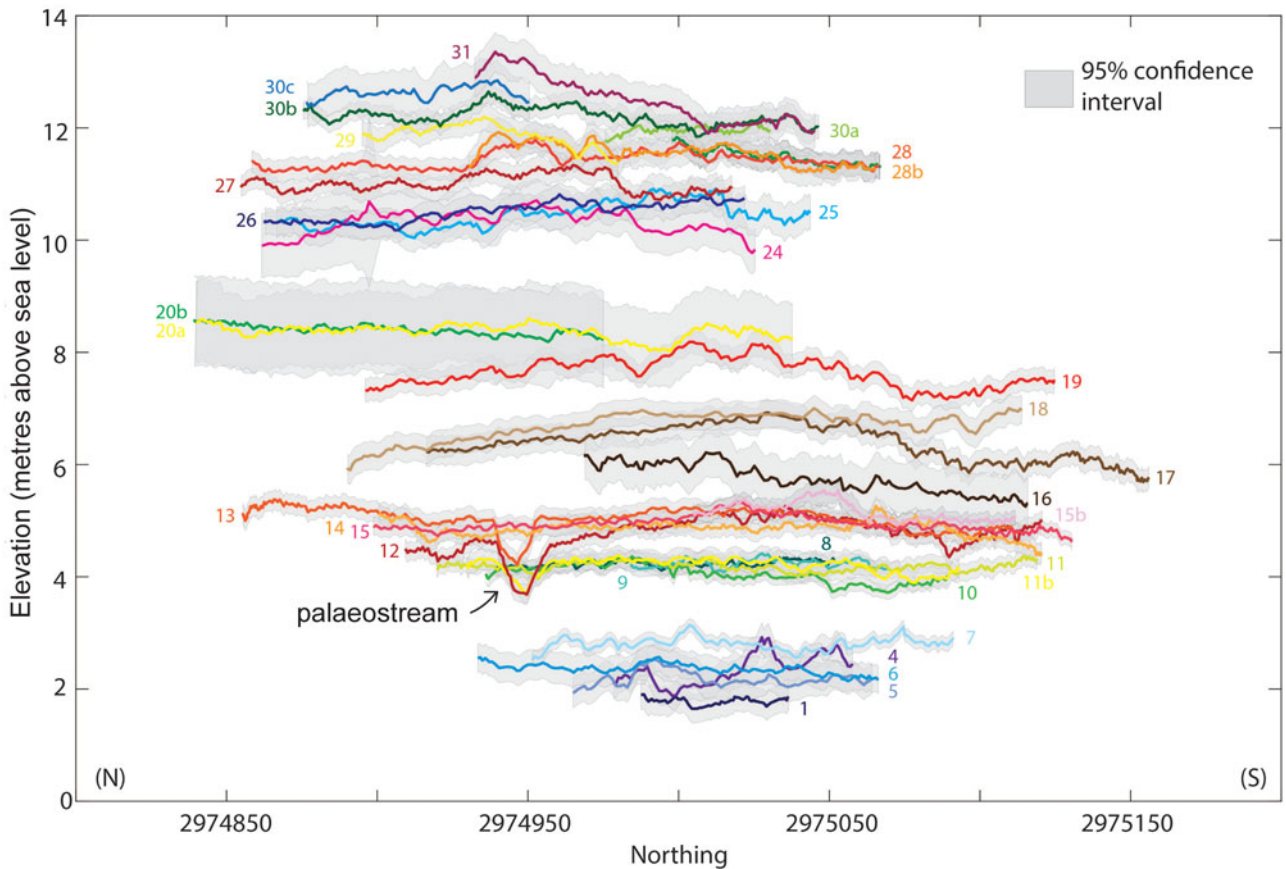


Fig. 4. Elevation transects across the crest of the most prominent beach ridges on Joinville Island. The 95% confidence intervals are shown by grey boxes. Not shown are beach ridges 2 and 3 due to limitations from local wildlife and beach ridges 21–23, whose GPS-processing error bars were so large as to obscure any meaningful results.

Software pulseEkko Pro with a 200 MHz antenna (Fig. 2; Zurbuchen & Simms 2019). Lines were predominantly collected shore-normal, with four additional shore-parallel profiles collected to help tie the other profiles together. The unshielded antenna was mounted on a custom-built cart and manually pulled across the beaches. Processing of the GPR profiles included a topographic correction, DeWow (a proprietary processing algorithm) and a depth-varying gain, all conducted using *EkkoDeluxe* and *Kingdom Suite* software. A velocity of 0.190 m/ns was used based on a common midpoint survey conducted at the site.

Beach age

Beach-ridge ages on Joinville Island were estimated using previously published radiocarbon ages in addition to 18 new optically stimulated luminescence (OSL) age determination attempts. Zurbuchen & Simms (2019) obtained radiocarbon ages for 18 of the lower 21 beach deposits (labelled 0–18, including 7a, 7b, 15a, 15b) on Joinville Island. With the exception of the ages from

beaches 1 and 2, which calibrate to < 448 years, these ages were recalibrated using *Calib* 8.2 (Heaton *et al.* 2020), with an updated marine radiocarbon reservoir offset (Delta R) of 695 ± 140 (Hall *et al.* 2010b; Calib.org/marine/regionalcalc.php, last accessed 16 August 2023). For the ages of beaches 1 and 2, we retained the ages originally used by Zurbuchen & Simms (2019), which were derived using a Bayesian progradation model for the beach-ridge age assignments. All ages in this study are given in calibrated years or thousands of years before present (the present being 1950). We use the notation 'cal. yr BP' to denote specific calibrated radiocarbon ages and 'ka' to represent time periods in the past and 'OSL ages' or 'kyr' for a span of time.

In order to supplement the previously reported radiocarbon ages by Zurbuchen & Simms (2019; <https://doi.org/10.1130/2019370>, last accessed 15 December 2022), cobbles and sands were sampled under lightproof conditions for OSL dating. We focused our efforts on the upper non-organic-bearing beaches. Sample preparation and OSL dating methods followed Simkins *et al.* (2016).

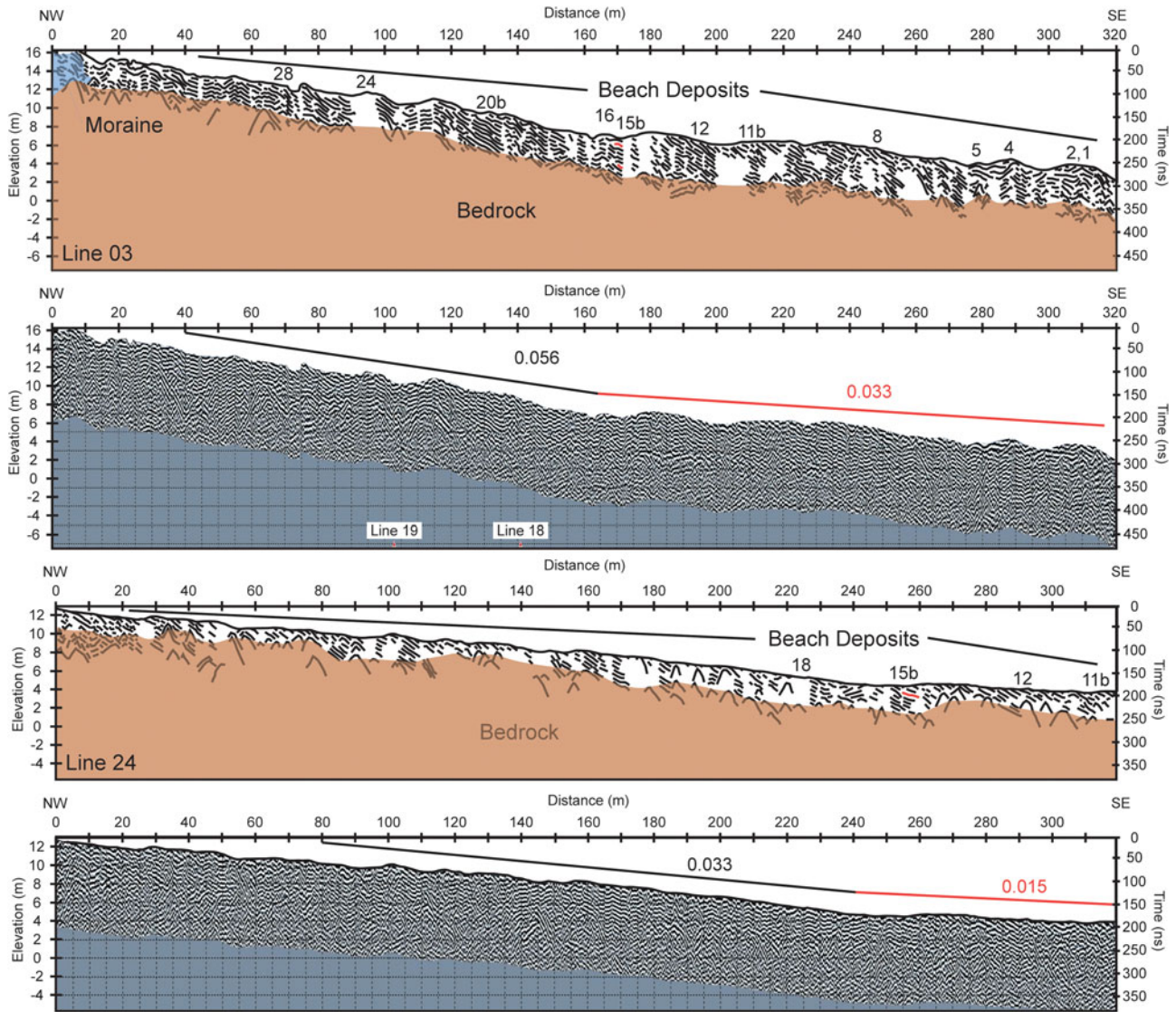


Fig. 5. Ground-penetrating radar (GPR) profiles and their interpretations for GPR lines 3 (upper two panels) and 24 (lower two panels). See Fig. 2 for GPR line locations.

The top, light-exposed portions were crushed for dose rate estimates. From the lower, light-shielded part of the cobble, the outer 1 mm surface was removed following Simms *et al.* (2011), who demonstrated that this layer was reset completely after 1 h of daylight exposure. The target slices were crushed by hand using a mortar and pestle in order to avoid pressures that could erase the luminescence signal. The carefully ground cobble grains and sediment from additional sandy deposits were prepared according to the following procedures: the material was sieved for grain sizes 63–250 μm . The grains were then washed in 10% HCl and 27% H_2O_2 to remove carbonate and organic material contaminants. The remaining sediment from sand and cobble samples was density separated with lithium polytungstate liquid (LST) at specific gravities of 2.75, 2.62, 2.58 and 2.54 to

isolate quartz, potassium and sodium feldspars and heavy and light grains. The heavy and light grains were saved and stored away, whereas the remaining quartz and feldspar grains were etched using hydrofluoric acid (48% HF for 40 min for quartz and 10% HF for 15 min for feldspars). Some samples had only little material in the feldspar fraction. For those samples, it was not possible to separate sodium and potassium feldspars. These samples were treated as 'mixed' feldspars.

Measurements were conducted using a Risø TL/OSL-DA-20 reader, Risø National Laboratory, with a bi-alkali photomultiplier tube (Thorn EMI 9635QB). The built-in $^{90}\text{Sr}/^{90}\text{Y}$ beta source gives a dose rate of ~ 100 mGy/s. The exact dose rate value was calculated for the specific day on which each sample was measured. For quartz, optical stimulation was carried out with a

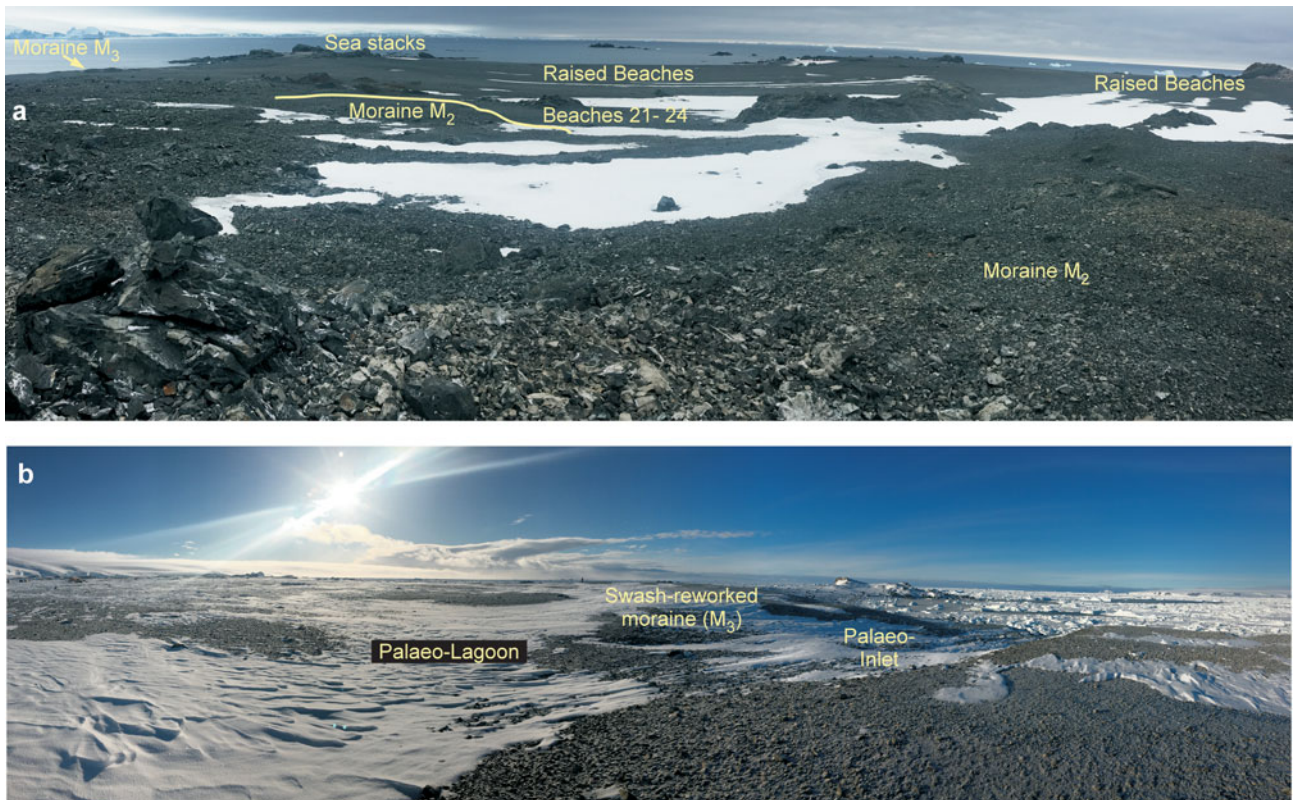


Fig. 6. a. Photograph looking east across Tay Head showing the relationship between the moraines and beaches as well as the character of M_2 . **b.** Photograph looking south-east into moraine M_3 and the possible palaeo-lagoon formed within it as it was reworked by swash processes.

blue LED array at 470 nm with 74 mW/cm² (90%) power at the sample and a 7.5 mm Hoya U-340 detection filter (290–370 nm). Feldspars were stimulated with an infrared LED array at 870 nm with 121 mW/cm² (90%) power at the sample and a blue or yellow filter combination for detection. The heating rate used was 5°C/s. Quartz grains did not have any significant luminescence signals. The measurement procedure for feldspar was based on the single-aliquot regenerative-dose (SAR) procedure described by Murray & Wintle (2000) and Wintle & Murray (2006). The procedure was modified such that the same temperature and 60 s duration were used for cutheat and preheat steps (compare Blair *et al.* 2007). The preheat temperatures were determined for each sample with plateau and dose recovery tests. The equivalent dose D_e was determined with the central age model (Galbraith 1999).

Calculation of the dose rate followed the procedure described in detail by Simms *et al.* (2011). Concentrations of natural uranium, ²³²Th and potassium were measured with high-resolution gamma-spectrometry for both rocks and surrounding material. All samples were in radioactive equilibrium. The water content for rocks was assumed to be 0. The water content for the surrounding materials was

measured and has an uncertainty of 3%. Alpha, beta and gamma dose rates were calculated using the conversion factors published by Guérin *et al.* (2011). The internal K concentrations in the feldspar samples (for single grains as well as average values) were measured with an electron

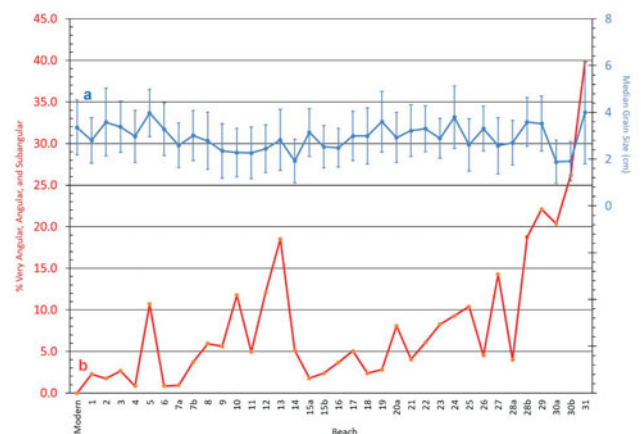


Fig. 7. a. Median long-axis grain size and **b.** the sum of the percentage of very angular, angular and subangular cobbles of the raised beaches at Tay Head, Joinville Island.

Table I. Granulometric characteristics of the raised beaches of Joinville Island.

Beach number	Grain size			Roundness						Clast type			
	Average (cm)	Median (cm)	Standard deviation (cm)	Very angular	Angular	Subangular	Sub-rounded	Rounded	Well-rounded	Total	OPP	Rhyolite	Sandstone ^a
Modern	3.52	3.35	1.17	0	0	0	3	39	61	103			
1	2.94	2.80	0.98	0	0	4	19	72	82	177	26	180	4
2	3.71	3.58	1.45	0	0	2	13	51	48	114	26	582	8
3	3.51	3.38	1.10	0	0	3	11	45	54	113	14	164	0
4	3.13	2.97	1.11	0	0	1	12	40	66	119			
5	4.03	3.97	1.01	0	0	11	35	38	19	103	41	448	2
6	3.53	3.28	1.13	0	0	1	21	50	47	119			
7a	2.72	2.59	0.95	0	0	1	19	41	46	107	23	220	2
7b	3.19	3.01	1.07	0	0	4	24	45	35	108			
8	2.97	2.78	1.22	0	0	6	23	34	38	101			
9	2.70	2.35	1.17	0	0	6	26	40	35	107	7	158	1
10	2.51	2.28	1.03	0	0	12	25	43	22	102			
11	2.53	2.27	1.11	0	0	5	19	48	29	101	24	350	3
12	2.60	2.44	1.02	0	0	11	32	30	18	91			
13	3.07	2.82	1.30	0	0	20	32	39	17	108	24	162	2
14	2.14	1.92	0.94	0	0	6	49	36	26	117			
15a	3.32	3.14	1.02	0	0	2	13	58	40	113	22	444	4
15b	2.57	2.53	0.91	0	0	3	33	61	29	126			
16	2.65	2.48	0.83	0	0	4	10	44	51	109			
17	3.16	2.99	1.06	0	0	6	13	56	44	119	25	513	1
18	3.18	2.99	1.20	0	0	3	24	52	47	126			
19	3.81	3.60	1.30	0	0	3	21	50	33	107	23	1048	2
20a	3.15	2.92	1.07	0	0	8	22	51	18	99			
21	3.34	3.22	1.11	0	0	5	26	46	46	123	23	36	3
22	3.39	3.30	0.98	0	1	5	16	50	27	99			
23	3.06	2.89	0.85	0	0	9	29	42	29	109	25	46	15
24	4.02	3.79	1.33	0	0	9	23	48	17	97			
25	2.83	2.61	1.12	0	0	13	32	55	25	125	15	96	35
26	3.48	3.30	0.96	0	0	5	34	61	11	111			
27	2.91	2.57	1.21	0	0	16	22	33	41	112	10	50	121
28a	2.85	2.70	0.95	0	0	4	10	46	40	100			
28b	3.78	3.59	1.04	0	3	18	30	47	14	112			
29	3.62	3.52	1.18	0	3	18	23	25	26	95	12	13	24
30a	2.03	1.88	0.92	0	1	22	37	44	9	113			
30b	2.11	1.91	0.84	0	6	22	19	50	10	107			
31	4.29	4.00	2.20	0	14	39	32	29	19	133	10	18	362
Moraine 3	-	-	-	0	16	24	22	36	27	125			

^a Probably an underestimate (see text).

OPP = out-of-place pebble.

probe micro-analyser (EPMA) at the University of California, Santa Barbara. To calculate the resulting internal dose rates, the grain sizes of the feldspars in the rock samples were measured. The cosmic dose rate was calculated as described by Barbouti & Rastin (1983), Prescott & Stephan (1982) and Prescott & Hutton (1994). The effective thickness was assumed to be half the burial depth. The uncertainty was 5%. Feldspar ages were fading corrected as described by Auclair *et al.* (2003) and Wallinga *et al.* (2007) for the linear and non-linear dose ranges, respectively.

Results

Beach-ridge architecture

Beach ridges appear to naturally clump into beach-ridge sets based on similar elevations, with what appear to be natural breaks between groups of three to seven beach ridges (Fig. 4). The lower beach-ridge sets include beaches 1–7 (GPR profiles reveal another break between beaches 2 and 3), 8–11b, 12–15b and 16–18. Above beach ridge ~20, the beach ridges became less continuous and more difficult to correlate across the beach plain. Nevertheless, natural breaks appeared to continue into the upper beach ridges, with more weakly developed breaks between beach-ridge sets defined by beach ridges 19–23, 24–27 and 28–31 (Fig. 2). The slope in the beach-ridge plain also changes at beach ~15b (Fig. 5). Along the profile of GPR line 3, orientated perpendicular to the beach ridges, above beach ridge 15b the slope is ~0.056, whereas below that it is ~0.033. The decrease is greater along GPR line 24, for which above beach ridge 15b the slope is ~0.033, whereas below that it is ~0.015.

Relationship between beaches and moraines

To the north of the raised beaches on Tay Head lie two to three moraines (Fig. 2; Simms *et al.* 2021). The oldest, M_1 , is located at the top (north-west) of the flight of raised beaches. M_1 appears to be overlapped or at least coeval with the highest beach ridges. Its well-rounded cobbles and smooth outer margin suggest reworking by marine processes, possibly into a palaeo-spit. Its interior may have been occupied by a palaeo-lagoon, which today occasionally fills with an ephemeral pond, complete with a palaeo-tidal inlet (Fig. 6). However, the palaeo-lagoon only contains coarse, angular cobbles with little to no mud.

To the north-east of M_1 lies another moraine or till sheet (M_2). It appears younger than M_1 , as M_2 's southern margin overrides some of the younger raised beaches (beaches 21–24; Fig. 6). The surface of M_2 is also hummocky (Fig. 6). Due to snow cover, the

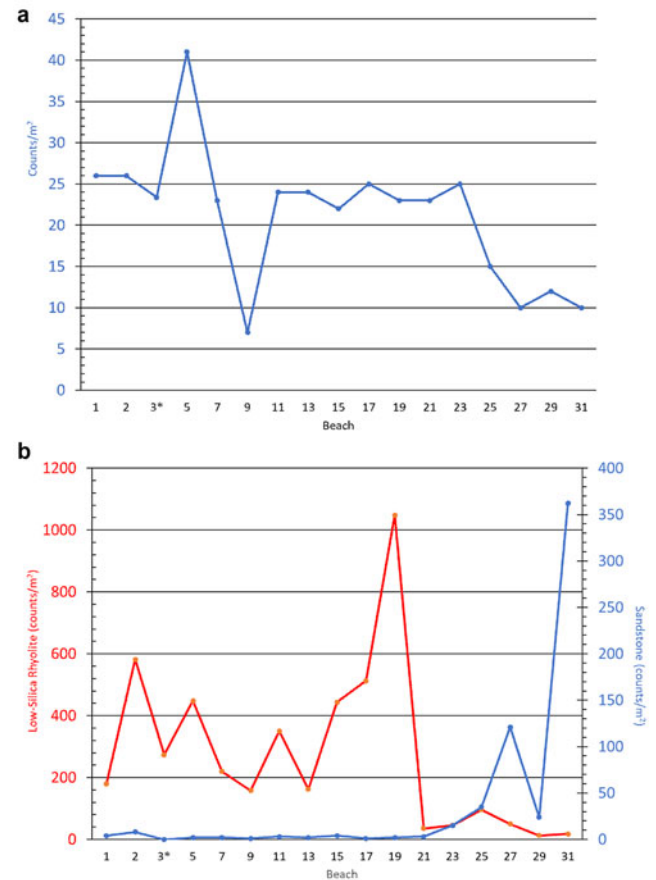


Fig. 8. a. Number of out-of-place pebbles (OPPs), interpreted as representing ice-rafted debris, per 1 m² of the beach for selected beaches on Tay Head, Joinville Island. Pebble counts were collected within 15 m² along the central portion of every other beach. **b.** Number of low-silica rhyolite (red) and sandstone (blue) pebbles per 1 m² of beach counted in the same manner as the OPP. *Pebbles were only counted on 9 m² of beach 3, thus the numbers presented have been normalized to 15 m². Note the frequency of sandstone pebbles is probably an underestimate (see text).

boundary between M_1 and M_2 was not clearly defined in the field, but it appears M_2 overlies M_1 . To the east of M_2 lies a third, younger moraine (M_3) described by Simms *et al.* (2021). M_3 appears to be younger than M_2 , as beaches 19 and 17 are cross-cut by M_3 but not clearly by M_2 . In addition, the cobbles within M_2 are much more angular compared to the more rounded cobbles of M_3 , which probably reworked older beach deposits (Simms *et al.* 2021).

Beach sedimentary characteristics

Based on 9092 grain-size measurements, the pebbles within Joinville Island's 36 beaches average between 2 and 4 cm in maximum length, with an overall standard

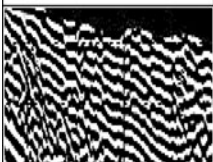

GPR Facies	Description	Interpretation
	Parallel to subparallel, seaward dipping (subhorizontal in strike profiles), semi-continuous reflections	Beach Deposits
	Chaotic, Prevalent hyperbolae	Bedrock

Fig. 9. Examples, descriptions and interpretations of ground-penetrating radar (GPR) facies #1 and #2.

deviation of 1.11 cm (Fig. 7 & Table I). Fine grains (e.g. diameters < 2 mm) were almost absent within the upper 15 cm of the beach deposits (Fig. 3). The mean grain size and sorting of pebbles on Joinville Island beaches did not change by > 1 cm across all of the beaches (Fig. 7). The oldest (19–31) and the youngest (modern-6) beaches contain some of the coarsest material and also vary considerably from the beaches

adjacent to them. The middle beaches (7–18) are slightly finer-grained, with less intra-beach variability. In addition, the sedimentary characteristics differed between the upper and lower beach deposits. The deposits of the lower 21 beaches (beach numbers 1–18, including 7b, 11b and the modern beach) were stratified with mats of seaweed within their matrix, whereas the deposits of the upper 15 beaches (beach numbers 19+) were not stratified and lacked seaweed (Fig. 3). Large, out-of-place (ice-rafted?) boulders also only occurred above beach ridge 20.

Roundness measurements performed on 4025 pebbles indicate the lower Joinville Island beaches are more rounded than the upper beaches (Fig. 7). Coarser grains are more easily rounded than finer grain sizes (cf. Boggs 2006), which could bias the roundness trends. However, after performing a permutation test on the data, the results failed to reject the null hypothesis of no correlation (Fig. S1), indicating grain size does not have an effect on the grain roundness of the Joinville Island beach deposits. Of the 36 beach deposits, nine modes are well rounded, 24 modes are rounded, two modes are sub-rounded and one mode is subangular (Table I). The general increase in pebble roundness through time is interrupted at beaches

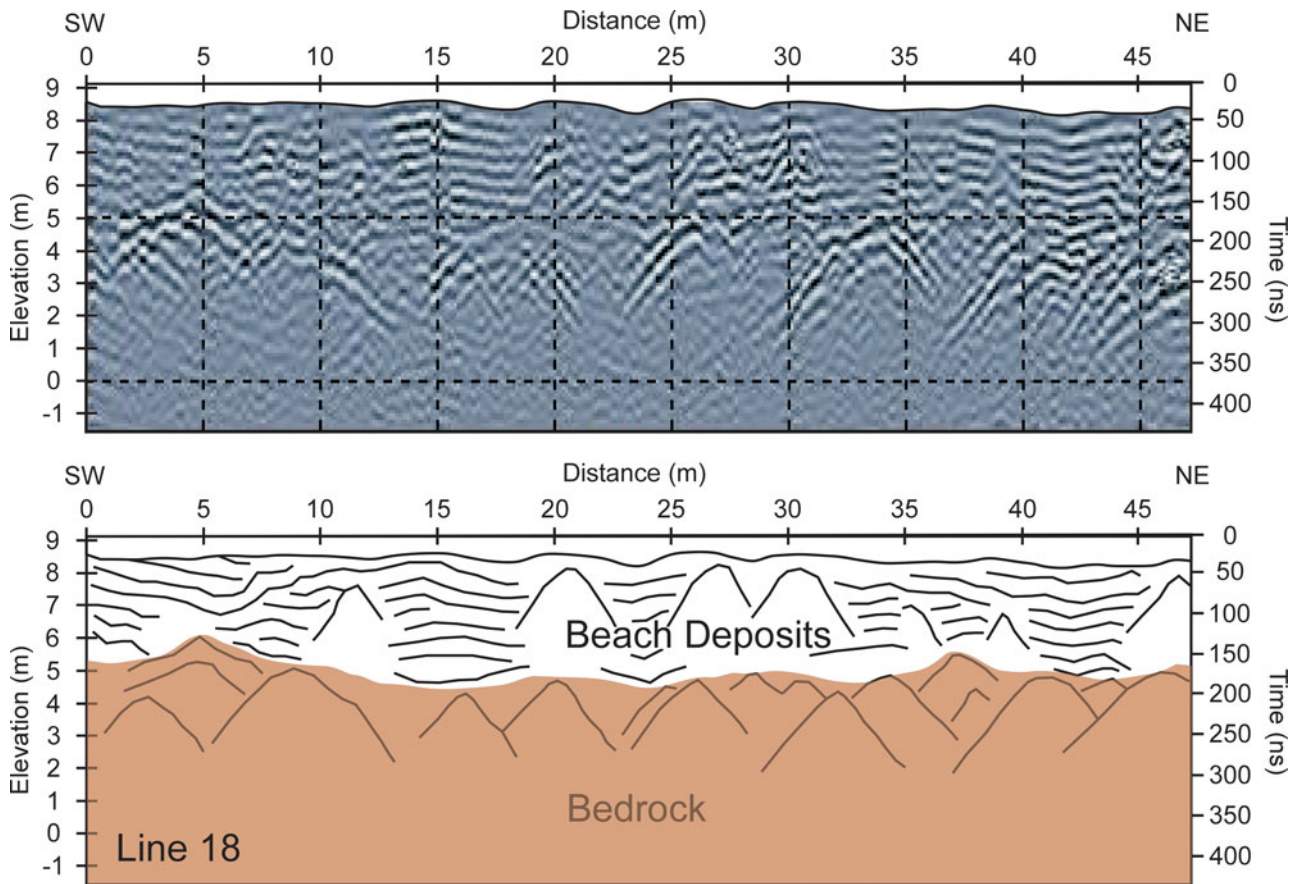


Fig. 10. Ground-penetrating radar (GPR) profile 8 and its interpretation. See Fig. 2 for the GPR line location.

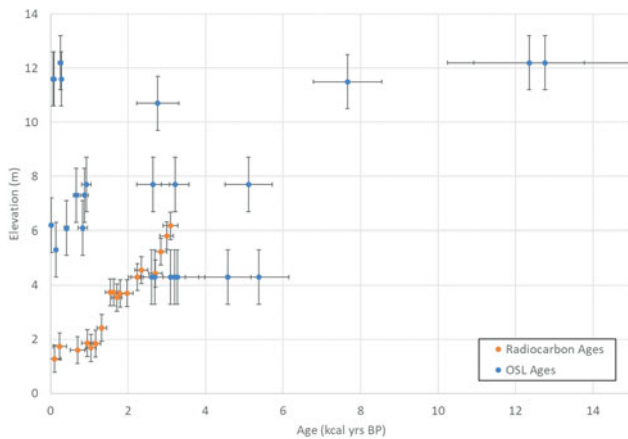


Fig. 11. Graph illustrating the height and age of beaches dated using optically stimulated luminescence (OSL) and radiocarbon dating.

5, 15, 16 and 28a (Fig. 7). Beach 5 exhibits less and beach 28a exhibits more rounding than the general trend (Fig. 7). Beach 5 is also one of the more coarse-grained beaches. The transition from beaches 15 to 14 indicates a decrease in pebble roundness over time, in opposition to the overall roundness trend.

The less-rounded deposits of beach 5 also have the most OPPs of any Joinville Island beach, whereas beach 9 has fewer OPPs than the surrounding beaches, and no changes in OPPs are seen through the transition from beaches 15 to 13 (Fig. 8). Unfortunately, OPP data were not directly counted for beach 28. In addition, the prevalence of more locally sourced rocks appears to change through time. Two of the most readily identifiable locally derived rock types observed while counting OPPs on Joinville Island were a low-silica rhyolite and sandstone/quartzite. Beaches 1–19 contained more low-silica rhyolite clasts, whereas beaches 21–31 contained less rhyolite and beaches 23–31 contained more sandstone clasts (Fig. 8).

Ground-penetrating radar survey results

The GPR profiles generally illustrate two dominant facies in the dip profiles. GPR facies #1 is composed of seaward-dipping, relatively continuous and parallel reflections (Fig. 9). In strike profiles, these regions are marked by flat-lying reflections (Fig. 10). GPR facies #2 is composed of chaotic, non-continuous, non-parallel reflections. Although hyperbolas are frequent throughout the data, they are most common at the interface between the two GPR facies and within GPR facies #2 (Fig. 10).

Onlap is common within reflections of GPR facies #1 and is most common along the boundary between sets of beach ridges (e.g. between beaches 2 and 3, 5 and 6, 7 and 8, 11b and 12, around 22, between 27 and 28, and

29 and 30). One of the most prominent areas of onlap corresponds with an overall change in the slope of the overall beach-ridge plain between beach ridges 15b and 18 (red reflection tracings in Fig. 5). At this location, the slope of the beach-ridge plain increases updip (Fig. 5).

Beach ages

Radiocarbon ages for the lower Joinville Island beaches were produced from shell and seaweed materials interbedded within the beach deposits, and the recalibrated ages range from 105 ± 160 (beach 1) to 3190 ± 375 cal. yr BP (beach 18), varying by < 100 years from their original calibration reported in Zurbuchen & Simms (2019; Fig. 11; <https://doi.org/10.1130/2019370>, last accessed 15 December 2022). OSL ages range from modern to $\sim 68.3 \pm 17$ ka (see the 'Discussion' section below). A summary of the samples and OSL ages is listed in Table II. Detailed results can be found in the Supplemental Materials (Tables S1 & S2). Out of 13 sediment samples, only seven had grain sizes in the range suited for OSL dating, whereas the others were too coarse. While 22 cobble surface samples were prepared, eight samples had no luminescence signal at all, even after irradiation with 100 Gy. Sand samples had generally brighter signals than cobble samples. Exceptions were the K-feldspar fractions of JV-26 and JV-32 ($\sim 10^6$ cps after 10 Gy irradiation). Dose recovery tests ranged from very good (> 5%) to medium (> 10%). The large overdispersion values (Table S2) are probably caused by the necessary crushing of the slices. Large grains with dose gradients inside the grain are broken into multiple pieces. Breakage inside grains instead of at grain boundaries leads to grains that consist of mineral mixtures. This is evidenced by the fact that grains in the Na-feldspar fraction were found to have comparatively high internal K concentrations (compare, for example, JV-27; Table S1). Fading rates had large measurement uncertainties due to the low signals and large differences between different aliquots of the same sample.

Discussion

Optically stimulated luminescence ages vs radiocarbon ages

Even when considering the challenging properties of the OSL samples, it is not fully clear why such a large discrepancy exists between the radiocarbon and OSL ages. We favour the radiocarbon ages over the OSL ages given their self-consistency (e.g. higher beach ridges return older ages and multiple ages from the same beach ridge are within error of one another) and agreement with regional records of RSL (e.g. Roberts *et al.* 2011). Some of the OSL samples (including JV17, JV27, JV32, SOSL JV-09 and SOSL-106) showed very good

Table II. Optically stimulated luminescence ages and sample properties.

Sample	Rock type	Mineral	Filter combi	Grain size (μm)	Dose (Gy)	DR total (Gy/year)	Age (ka)	Beach height (m)	Beach number
JV-10	Fractured hornblende, granodiorite	Mixed feldspar	Blue	63–250	11.22 ± 3.06	4.63 ± 1.04	3.3 ± 1.3	4.3	12
JV-13	Biotite-hornblende, tonalite	Mixed feldspar	Blue	63–500	8.83 ± 0.75	3.96 ± 0.65	2.77 ± 0.55	10.7	28
JV-14	Biotite, hornblende, tonalite	Mixed feldspar	Blue	63–500	0.85 ± 0.067	4.40 ± 0.72	0.257 ± 0.56	12.2	31
JV-15	Biotite, hornblende, granite	K-feldspar	Blue	63–500	1.52 ± 0.13	5.49 ± 0.53	0.277 ± 0.036	11.6	30
JV-16	Hornblende, tonalite	K-feldspar	Blue	63–212	6.35 ± 0.26	7.91 ± 0.83	0.92 ± 0.12	7.7	20
JV-17	Hornblende, quartz, monzonite	K-feldspar	Yellow	63–250	3.00 ± 0.15	4.54 ± 0.45	0.661 ± 0.074	7.3	19
JV-20	Hornblende, tonalite	Na-feldspar	Yellow	63–250	4.18 ± 0.18	4.76 ± 0.46	0.878 ± 0.093	5.3	16
JV-22	Hornblende, granite	Mixed feldspar	Blue	63–250	0.195 ± 0.022	2.22 ± 0.37	0.141 ± 0.035	6.2	18
JV-22		K-feldspar	Blue	63–250	0.083 ± 0.004	6.80 ± 0.76	0.012 ± 0.001		
JV-22		Na-feldspar	Yellow	63–250	0.059 ± 0.004	3.71 ± 0.39	0.016 ± 0.002		
JV-23	Biotite, hornblende, tonalite	K-feldspar	IR/blue	63–500	3.95 ± 0.16	5.53 ± 0.60	0.831 ± 0.12	6.1	17
JV-23		Na-feldspar	Yellow	63–500	1.04 ± 0.068	4.49 ± 0.49	0.413 ± 0.061		
JV-26	Biotite, hornblende, tonalite	K-feldspar	Blue	63–500	0.295 ± 0.023	5.34 ± 0.65	0.068 ± 0.036	11.6	30
JV-26		Na-feldspar	Blue	63–212	0.156 ± 0.019	3.77 ± 0.43	0.087 ± 0.02		
JV-26		K-feldspar	Blue	63–250	21.04 ± 0.84	7.63 ± 0.68	3.21 ± 0.36		
JV-27	Hornblende, granite	Na-feldspar	Yellow	63–250	11.04 ± 0.42	5.37 ± 0.60	2.65 ± 0.42	7.7	20
JV-27		K-feldspar	Blue	63–250	21.04 ± 0.84	7.63 ± 0.68	3.21 ± 0.36		
JV-30	Tonalite	Mixed feldspar	Blue	63–500	245 ± 16	7.58 ± 0.74	27.2 ± 3.2	6.1	17
JV-32	Hornblende, granite	K-feldspar	Blue	63–500	32.2 ± 1.6	7.26 ± 0.70	5.11 ± 0.61	7.7	20
JV-34	Sandstone?	Mixed feldspar	Blue	63–500	171 ± 24	3.38 ± 0.28	68 ± 17	10.7	28
SOSL JV-07		Mixed feldspar	Blue	90–212	9.57 ± 0.65	3.09 ± 0.15	5.38 ± 0.78	4.3	12
SOSL JV-09		K-feldspar	Blue	63–212	8.00 ± 0.34	3.47 ± 0.31	3.09 ± 0.38	4.3	12
SOSL JV-09		K-feldspar	Yellow	63–212	8.17 ± 0.38	3.47 ± 0.31	2.69 ± 0.47		
SOSL JV-09		Na-feldspar	Blue	63–212	6.84 ± 0.55	3.16 ± 0.16	3.21 ± 0.62		
SOSL-101		Na-feldspar	Yellow	63–212	6.76 ± 0.35	3.16 ± 0.16	2.61 ± 0.3	12.2	31
SOSL-101		Mixed feldspar	Blue	90–212	22.7 ± 1.5	3.40 ± 0.15	12.8 ± 2.5		
SOSL-102		Mixed feldspar	Blue	90–212	31.2 ± 2.2	3.53 ± 0.19	12.4 ± 1.4	12.2	31
SOSL-104		Mixed feldspar	Blue	90–212	57.3 ± 3.6	3.46 ± 0.17	25.6 ± 4.3	11.5	29
SOSL-106		Mixed feldspar	Blue	90–212	51.2 ± 3.1	3.69 ± 0.20	23.1 ± 3.4	11.5	29
SOSL-107		K-feldspar	Blue	90–212	19.1 ± 1.1	3.39 ± 0.17	7.66 ± 0.88	11.5	29

All samples labelled 'JV-x' are rock samples. Samples labelled SOSL-x are sediment samples.

Minerals: for samples with sufficient materials, feldspars were separated into K-feldspar (< 2.58 SG) and Na-feldspar (> 2.58 SG). For all other samples, the fraction < 2.62 SG was labelled as 'mixed' feldspars.

Filter combi: in general, the brightest signal was used for dating. For most mixed feldspars and K-feldspars this was the blue signal, whereas Na-feldspars were brighter in yellow. There are some exceptions, as listed.

Grain size: the grain size was obtained after sifting of sediments or after crushing and sifting of rock slices.

Age: the final age, after fading correction where applicable.

Beach height: the height of the beach in metres where the sample was collected.

DR = dose rate; IR = infrared.

luminescence properties: very good dose recovery, low overdispersion values and small uncertainties for the fading rates. For some of the samples (JV17, JV27, SOSL JV-09), ages were measured with both K-Feldspar and Na-feldspar fractions, and the two independent results agree in each case within 1-sigma error limits. Yet the OSL ages show little to no agreement with the

radiocarbon ages. Four beaches (beaches 12 and 16–18) were sampled by both OSL and radiocarbon dating. Of those, only OSL ages from beach ridge 12 fall within error of the radiocarbon ages (Fig. 11). All ages except one from beaches 16–18 returned anomalously young ages, possibly reflecting exposure after ridge formation. The other age is much older than expected (Table II).

The ages from the higher beach ridges appear to suffer from similar uncertainties, with seven of the 17 ages dating to < 500 years old despite probably being older than 3 ka based on the radiocarbon ages. Similarly, three others are younger than ~3 ka, despite being higher than the 3 ka-old beaches based on the radiocarbon ages. Three more OSL ages are anomalously old at ~68, 27 and 25 ka and may reflect incomplete resetting during their last exposure. Two separate ages obtained from the same beach ridge date to an apparently anomalously old age of 12 ka, but they appear correct based on their OSL characteristics. Their age is intriguing but probably too old based on the glacial history of the region (Michalchuk *et al.* 2009). That leaves two ages that fit the general RSL trend of the younger radiocarbon-based chronology: JV-32, with an age of 5.1 ± 0.6 ka from beach 20 at an elevation of 7.7 m, and SOSL-107, with an age of 7.7 ± 0.9 ka from beach 29 at an elevation of 11.5 m. Assuming an average rate of beach formation of 175 years, based on the frequency of the lower ^{14}C -dated beaches, the age of beach 31 is expected to be older than 5.8 ka, and accounting for hiatuses would probably make the section older.

Neoglacial and beach architecture

Several shifts in beach characteristics are observed in the beaches of Tay Head, but the largest and most pronounced change occurs around beaches 15a and 15b. At this point, the slope of the larger beach plain decreases (Fig. 5), and it is near the onset of seaweed preservation and the development of well-defined stratification within the beaches (beach 18), although we cannot rule out the possibility that the change in fabric is due to post-depositional changes (e.g. frost processes) to the upper beach ridges. Adjacent beach ridge 15a also marks a significant interruption in the general increase in pebble roundness through time (Fig. 7). The age of beaches 15a and 15b (~2.7 ka) corresponds to the onset of the well-documented Neoglacial time period between ~2.1 and ~2.5 ka (Bentley *et al.* 2009, Cejka *et al.* 2020). Pronounced cooling on James Ross Island supports the onset of the Neoglacial period at 2.5 ka (Mulvaney *et al.* 2012, Totten *et al.* 2015, Kaplan *et al.* 2020), although some proxies, such as those from a SHALDRIL core taken in the Firth of Tay (Michalchuk *et al.* 2009) and the Palmer Deep Site 1098 on the western AP (Domack 2002, Shevenell & Kennett 2002, Shevenell *et al.* 2011), suggest that the Neoglacial period initiated earlier, at closer to 3.5 ka, whereas others along the EAP suggest the Neoglacial period to be younger (Cejka *et al.* 2020). Along Tay Head, prolonged cooling associated with the Neoglacial time period could have increased sea-ice conditions and hindered clast rounding,

leading to a decrease in pebble roundness, but this did not close the sea off enough to prevent icebergs from landing on the shore. Additionally, cooling may have driven localized glacier readvance (see below) and potentially increased sediment supply to the coast. An increased sediment supply could have led to the introduction of more angular beach clasts and a change in shoreline trajectory, leading to the lower slopes of the beach plain.

Other changes in Joinville Island beaches and their pebble roundness

In addition to the major change centred around beach ridge 15b at 2.7 ka, beach sets on Tay Head show breaks within the last ~0.7 kyr (the break between beaches 2 and 3), ~1.4 ka (beaches 7 and 8), ~2.1 ka (beaches 11b and 12) and sometime after ~3.2 ka with the age of the older breaks above beach 18, with the exception of the break between beaches 27 and 28 at ~7.5 ka, being poorly constrained. The younger events appear to coincide with glacial advances on the western AP documented by overridden mosses at ~0.2, ~0.8 and ~1.2 ka (Groff *et al.* 2023). Zurbuchen & Simms (2019) suggest that the breaks at ~1.4 and ~2.1 ka were the result of increases in the rate of RSL fall due to glacial isostatic adjustment-driven uplift. The others may be driven by a similar process. Interestingly, the events at ~1.4 and ~2.7 ka correspond to Bond events #1 and #2 (Bond *et al.* 1992).

In addition to the large interruption in beach pebble roundness as a potential result of the Neoglacial, the overall increase in beach pebble roundness through time on Joinville Island was interrupted at beaches 5 and 28a (Fig. 7). These interruptions do not correlate with inferred RSL changes described by Zurbuchen & Simms (2019), which suggests that these differences were caused by factors other than changes in the rate of RSL. Beach 5 contains less rounded materials and formed 1005 ± 310 cal. yr BP. The formation of beach 5 corresponds in timing with a negative Southern Hemisphere Annular Mode (SAM) event, which marks cooler climate conditions as the southern westerlies probably shifted towards the equator (Kwok & Comiso 2002, Moreno *et al.* 2018, Kaplan *et al.* 2020). The temperature anomaly record from the James Ross Island ice core (Mulvaney *et al.* 2012) supports this suggestion, as temperatures were low at the time and continued to decrease thereafter. Additionally, anomalously low pebble roundness values are also found in Marguerite Bay (Simkins *et al.* 2015) at the same time as the formation of Joinville Island beach 5. Thus, the reduced rounding of sediments within beach 5 could be the result of a widespread period of less open water conditions, with an increase in sea ice observed in the relative

abundance of diatom assemblages in other marine records (Barbara *et al.* 2016), indicative of cooler temperatures. Additionally, beach 5 has the highest OPP count, interpreted as representing IRD, which further supports the importance of cooler temperatures during the formation of beach 5. Cooler temperatures might have led to a glacial advance on Joinville Island and/or surrounding regions and supplied more icebergs carrying IRD (Bond *et al.* 1992). According to Mulvaney *et al.* (2012), a permanent ice shelf formed after ~ 1.5 ka within the Prince Gustav Channel, which offers a potential source of IRD for beach 5. Additionally, ice advances on James Ross Island (Björck *et al.* 1996, Kaplan *et al.* 2020) and nearby islands (Balco & Schaefer 2013) occurred at or after 1.4 ka.

Finally, beach 28a had more rounded beach materials compared to the overall roundness trend (Fig. 7). Increased pebble roundness could reflect higher wave exposure, suggestive of less sea-ice coverage. The second beach above beach 28a, beach 29, has an OSL age of 7.7 ± 0.9 ka. If the average rate of beach formation is ~ 175 years, then that would suggest an age of ~ 7.4 ka for beach 28. Marine records from the neighbouring Firth of Tay (Majewski & Anderson 2009, Michalchuk *et al.* 2009) suggest the onset of warmer and more open water conditions at about this time. At ~ 7.8 ka, Michalchuk *et al.* (2009) observed a distinct change in the marine sediments of the Firth of Tay, with an increase in diatoms, organic carbon, nitrogen and biogenic silica and a decrease in IRD. However, similar signals are not ubiquitous throughout the region (e.g. Shevenell *et al.* 2011, Mulvaney *et al.* 2012, Barbara *et al.* 2016).

Joinville Island glacial advance

The increase in low-silica rhyolite and the decrease in sandstone clasts with time on the beaches of Tay Head could be manifestations of a change in beach sediment provenance. Outcrops of the sandstone are located west of the three moraines or till sheets, whereas the low-silica rhyolite was present as dikes within low-grade, metamorphosed, fine-grained sedimentary rocks in the sea stacks and outcrops on the eastern side of Tay Head (Fig. 2). The rocks within the westernmost M_1 moraine behind beach 31 were dominantly sandstone. Therefore, the sediment sources for the upper beaches (21–31) were most probably the moraine and sandstone outcrops to the east, and, as beaches became preserved, eventually the sandstone sources were abandoned or swamped by materials from other parts of the peninsula. Subsequently, the dominant sediment source transitioned to the low-grade, metamorphosed, fine-grained sedimentary rocks with the low-silica rhyolite dykes for the lower beaches. However, this transition does not align with

changes in pebble roundness, indicating that processes other than just a source change caused the changes in pebble roundness. Although the age of the westernmost moraine M_3 is unknown, beach 31 cuts into the moraine, suggesting that it is older than 7.7 ka.

Two other moraines or till sheets are present north of the beaches on Tay Head (M_2 and M_3 ; Fig. 2). The sandstone would have been transported east by glacial ice to form the upper moraine (M_1) and hence sourced the upper beaches (21–31). The low-silica rhyolite and its affiliated low-grade, metamorphosed, fine-grained sedimentary rocks are present in the area. The easternmost two moraines appeared to be composed of these rocks. The middle of the two moraines, M_2 , cuts across beaches 21–24, which we estimate to be 175–525 years older than beach 20, which has an OSL age of 5.1 ± 0.6 ka; whereas the lower moraine, M_3 , cuts across beaches 12 and possibly beach 8, thus post-dating ~ 1.5 ka BP as reported by Simms *et al.* (2021). However, we cannot rule out the possibility that M_2 and M_3 represent the same advance but with a very irregular margin.

Conclusion

Changes in the sediment characteristics as revealed in GPR profiles, grain size, grain roundness and IRD within Holocene raised beaches on Joinville Island along the EAP were used to determine how the environmental history of the region is reflected within their deposits. A particularly well-developed set of 36 raised beaches is found on Tay Head on the southern side of Joinville Island. The lower 21 beaches are well stratified and better developed than the upper 15 beaches, which are unstratified and less contiguous. Furthermore, most beaches are found in sets of three to seven beach ridges separated from other beach-ridge sets by natural breaks in elevation without beach ridges. Grains on the raised beaches of Joinville Island show an overall increase in beach pebble roundness through time, whereas grain size shows no obvious pattern. However, the pebble roundness trend is interrupted at beaches 5, 15a and 28a. Beach 5 exhibits less and beach 28a exhibits more rounding than the general trend. The transition between beaches 15 and 14 indicates a sharp decrease in pebble roundness through time, in opposition to the overall pebble roundness trend. The change in roundness trend is also nearly concurrent with an inflection point in the overall slope of the beach plain and observable onlapping in GPR profiles. The lower 21 beaches contain prevalent seaweed mats and limpet shells, providing an excellent radiocarbon chronology. An attempt to date four of the lower radiocarbon-dated beaches and five of the upper beaches with 21 OSL ages from cobble surfaces as well as more traditional sand

grains was met with mixed success. The age of beaches 15a and 15b (~2.7 ka), which marked a transition in pebble roundness of the beaches as well as a lowering of the overall beach plain slope, coincides with the onset of the Neoglacial time period of ~2.5–3.0 ka. Less rounding of sediments within the ~1.0 ka beach 5, which also had the most OPPs (interpreted as representing IRD) of any beach on Joinville Island, could be explained by a period marked by shorter open water seasons and an increase in sea ice, whereas the opposite could hold true for beach 28a of ~7.4 ka. This study suggests Holocene environmental changes left a measurable impact on the coastal zones of Antarctica.

Acknowledgements

We would like to thank Cara Ferrier and Laura Reynolds for their help in the field. We would also like to thank the captains and crews of the *Lawrence M. Gould* and *Almirante Irazar*, without whose help we would still be on Joinville Island. Aidan Patterson helped with grain size and shape characterization. Gareth Seward performed EPMA measurements of feldspar separates. Claire Divola helped draft Fig. 4. We would also like to thank Daniel Nývlt and an anonymous reviewer for their constructive comments that helped improve the manuscript.

Financial support

This work was supported through National Science Foundation (NSF) grant 0724929 to ARS and RD. Additional support was provided by a Geological Society of America Graduate Student Research Grant and an NSF Graduate Research Fellowship to JZ.

Author contributions

ARS and RD designed the experiment. ARS, JZ and CGa conducted the fieldwork. ARS and JZ conducted the ground-penetrating radar analysis. BMT conducted the grain size and roundness analysis as well as the ice-rafted debris counting and initial interpretations. BMT, RD, CGa and CGe conducted the optically stimulated luminescence analysis. BMT and ARS wrote the manuscript with input from RW, CGe and the rest of the authors.

Supplementary materials

Two supplemental tables and a supplemental figure will be found at <https://doi.org/10.1017/S0954102023000275>.

References

AMBROZOVA, K., LASKA, K. & KAWAN, J. 2020. Multi-year assessment of atmospheric circulation and impacts on air temperature variation on

- James Ross Island, Antarctic Peninsula. *International Journal of Climatology*, **40**, 1526–1541.
- AMBROZOVA, K., LASKA, K., HRBACEK, F., KAWAN, J. & ONDRUCH, J. 2019. Air temperature and lapse rate variation in the ice-free and glaciated areas of northern James Ross Island, Antarctic Peninsula, during 2013–2016. *International Journal of Climatology*, **39**, 643–657.
- AUCLAIR, M., LAMOTHE, M. & HUOT, S. 2003. Measurement of anomalous fading for feldspar IRSL using SAR. *Radiation Measurements*, **37**, 487–492.
- BALCO, G. & SCHAEFFER, J.M. 2013. Exposure-age record of Holocene ice sheet and ice shelf change in the northeast Antarctic Peninsula. *Quaternary Science Reviews*, **59**, 101–111.
- BARBARA, L., CROSTA, X., LEVENTER, A., SCHMIDT, S., ETOURNEAU, J., DOMACK, E. & MASSÉ, G. 2016. Environmental responses of the northeast Antarctic Peninsula to the Holocene climate variability. *Paleoceanography*, **31**, 131–147.
- BARBEAU, D.L. JR, DAVIS, J.T., MURRAY, K.E., VALENCIA, V., GEHRELS, G.E., ZAHID, K.M. & GOMBOSI, D.J. 2010. Detrital-zircon geochronology of the metasedimentary rocks of north-western Graham Land. *Antarctic Science*, **22**, 65–78.
- BARBOUTI, A. & RASTIN, B. 1983. A study of the absolute intensity of muons at sea level and under various thicknesses of absorber. *Journal of Physics G: Nuclear Physics*, **9**, 1577–1595.
- BENTLEY, M., HODGSON, D., SMITH, J. & COX, N. 2005. Relative sea level curves for the South Shetland Islands and Marguerite Bay, Antarctic Peninsula. *Quaternary Science Reviews*, **24**, 1203–1216.
- BENTLEY, M., HODGSON, D., SMITH, J., COFAIGH, C., DOMACK, E., LARTER, R., *et al.* 2009. Mechanisms of Holocene palaeoenvironmental change in the Antarctic Peninsula region. *The Holocene*, **19**, 51–69.
- BJÖRCK, S., OLSSON, S., ELLIS-EVANS, C., HÅKANSSON, H., HUMLUM, O. & DE LIRIO, J.M. 1996. Late Holocene palaeoclimatic records from lake sediments on James Ross Island, Antarctica. *Palaeoecology, Palaeoclimatology, Palaeoecology*, **121**, 195–220.
- BLAIR, M.W., KALCHGRUBER, R. & MCKEEVER, S.W.S. 2007. Developing luminescence dating for extraterrestrial applications: characterization of Martian simulants and minerals. *Radiation Measurements*, **42**, 392–399.
- BOGGS, S. JR. 2006. *Principles of sedimentology and stratigraphy*, 4th edition. Hoboken, NJ: Pearson Prentice Hall, 688 pp.
- BOND, G., HEINRICH, H., BROECKER, W., LABEYRIE, L., MC MANUS, J., ANDREWS, J., *et al.* 1992. Evidence for massive discharges of icebergs into the North Atlantic ocean during the last glacial period. *Nature*, **360**, 245.
- BRADSHAW, J.D., VAUGHAN, A.P.M., MILLAR, I.L., FLOWERDEW, M.J., TROUW, R.A.J., FANNING, C.M. & WHITESHOUSE, M.J. 2012. Permo-carboniferous conglomerates in the Trinity Peninsula Group at View Point, Antarctic Peninsula: sedimentology, geochronology and isotope evidence for provenance and tectonic setting in Godwana. *Geological Magazine*, **149**, 626–644.
- BUTLER, E.R. 1999. Process environments on modern and raised beaches in McMurdo Sound, Antarctica. *Marine Geology*, **162**, 105–120.
- CARRIVICK, J.L., DAVIES, B.J., GLASSER, N.F., NYVLT, D. & HAMBREY, M.J. 2012. Late-Holocene changes in character and behaviour of land-terminating glaciers on James Ross Island, Antarctica. *Journal of Glaciology*, **58**, 1176–1190.
- CEJKA, T., NYVLT, D., KOPALOVA, K., BULINOVA, M., KAWAN, J., LIRIO, J.M., *et al.* 2020. Timing of the neoglacial onset on the north-eastern Antarctic Peninsula based on lacustrine archive from Lake Anonima, Vega Island. *Global and Planetary Change*, **184**, 103050.
- CHARMAN, D.J., AMESBURY, M.J., ROLAND, T.P., ROYLES, J., HODGSON, D.A., CONVEY, P. & GRIFFITHS, H. 2018. Spatially coherent late Holocene Antarctic Peninsula surface air temperature variability. *Geology*, **46**, 1071–1047.
- DAVIES, B.J., GOLLEDGE, N.R., GLASSER, N.F., CARRIVICK, J.L., LIGTENBERG, S.R., BARRAND, N.E., *et al.* 2014. Modelled glacier response to centennial temperature and precipitation trends on the Antarctic Peninsula. *Nature Climate Change*, **4**, 993–998.

- DICKENS, W.A., KUHN, G., LENG, M.J., GRAHAM, A.G.C., DOWDESWELL, J.A., MEREDITH, M.P., *et al.* 2019. Enhanced glacial discharge from the eastern Antarctic Peninsula since the 1700s associated with a positive southern Annular Mode. *Scientific Reports*, **9**, 14606.
- DOMACK, E.W. 2002. A synthesis for site 1098: Palmer Deep. *Proceedings of the Ocean Drilling Program, Scientific Results*, **178**, 77843–79547.
- DOMACK, E.W. & MCCLENNEN, C.E. 1996. Accumulation of glacial marine sediments in fjords of the Antarctic Peninsula and their use as late Holocene paleoenvironmental indicators. *Foundations for Ecological Research West of the Antarctic Peninsula*, **70**, 135–154.
- DOMACK, E.W., ISHMAN, S.E., STEIN, A.B., MCCLENNEN, C.E. & JULL, A.T. 1995. Late Holocene advance of the Müller Ice Shelf, Antarctic Peninsula: sedimentological, geochemical and palaeontological evidence. *Antarctic Science*, **7**, 159–170.
- DOMACK, E.W., LEVENTER, A., DUNBAR, R., TAYLOR, F., BRACHFELD, S. & SJUNNESKOG, C. 2001. Chronology of the Palmer Deep site, Antarctic Peninsula: a Holocene paleoenvironmental reference for the circum-Antarctic. *The Holocene*, **11**, 1–9.
- DOMACK, E.W., LEVENTER, A., ROOT, S., RING, J., WILLIAMS, E., CARLSON, D., *et al.* 2003. Marine sedimentary record of natural environmental variability and recent warming in the Antarctic Peninsula. *Antarctic Peninsula Climate Variability: Historical and Paleoenvironmental Perspectives*, **79**, 205–224.
- ELLIOT, D. 1967. The geology of Joinville Island. *BAS Bulletin*, No. **12**, 23–40.
- EVANS, J., PUDSEY, C.J., ÓCOFAIGH, C., MORRIS, P. & DOMACK, E. 2005. Late Quaternary glacial history, flow dynamics and sedimentation along the eastern margin of the Antarctic Peninsula Ice Sheet. *Quaternary Science Reviews*, **24**, 741–774.
- GALBRAITH, R.F., ROBERTS, R.G., LASLET, G.M., YOSHIDA, H. & OLLEY, J.M. 1999. Optical dating of single and multiple grains of quartz from Jinnium rock shelter, northern Australia: part I, experimental design and statistical models. *Archaeometry*, **41**, 339–364.
- GARCÍA, M., CASTRO, C.G., RIOS, A., DOVAL, M.D., ROSÓN, G., GOMIS, D. & LÓPEZ, O. 2002. Water masses and distribution of physico-chemical properties in the Western Bransfield Strait and Gerlache Strait during austral summer 1995/96. *Deep-Sea Research II*, **49**, 585–602.
- GLASSER, N.F., DAVIES, B.J., CARRIVICK, J.L., RODES, A., HAMBREY, M.J., SMELLIE, J.L. & DOMACK, E. 2014. Ice-stream initiation, duration and thinning on James Ross Island, northern Antarctic Peninsula. *Quaternary Science Reviews*, **86**, 78–88.
- GROFF, D.V., BEILMAN, D.W., YU, Z., FORD, D. & XIA, Z. 2023. Kill dates from re-exposed black mosses constrain past glacier advances in the northern Antarctic Peninsula. *Geology*, **51**, 257–261.
- GUÉRIN, G., MERCIER, N. & ADAMIEC, G. 2011. Dose-rate conversion factors: update. *Ancient TL*, **29**, 5–8.
- GUGLIELMIN, M., CONVEY, P., MALFASI, F. & CANNONE, N. 2016. Glacial fluctuations since the 'Medieval Warm Period' at Rothera Point (western Antarctic Peninsula). *The Holocene*, **26**, 154–158.
- HALL, B. 2007. Late-Holocene advance of the Collins Ice Cap, King George Island, South Shetland Islands. *The Holocene*, **17**, 1253–1258.
- HALL, B. 2009. Holocene glacial history of Antarctica and the sub-Antarctic islands. *Quaternary Science Reviews*, **28**, 2213–2230.
- HALL, B. 2010. Holocene relative sea-level changes and ice fluctuations in the South Shetland Islands. *Global and Planetary Change*, **74**, 15–26.
- HALL, B. & PERRY, E.R. 2004. Variations in ice rafted detritus on beaches in the South Shetland Islands: a possible climate proxy. *Antarctic Science*, **16**, 339–344.
- HALL, B., KOFFMAN, T. & DENTON, G. 2010a. Reduced ice extent on the western Antarctic Peninsula at 700–970 cal. yr BP. *Geology*, **38**, 635–638.
- HALL, B., HENDERSON, G.M., BARONI, C. & KELLOGG, T.B. 2010b. Constant Holocene Southern-Ocean ¹⁴C reservoir ages and ice-shelf flow rates. *Earth and Planetary Science Letters*, **296**, 115–123.
- HEATON, T.J., KOHLER, P., BUTZIN, M., BARD, E., REIMER, R.W., AUSTIN, W.E.N., *et al.* 2020. Marine20 - the marine radiocarbon age calibration curve (0–55,000 cal BP). *Radiocarbon*, **62**, 779–820.
- HODGSON, D.A. & CONVEY, P. 2005. A 7000-year record of oribatid mite communities on a maritime-Antarctic island: responses to climate change. *Arctic, Antarctic, and Alpine Research*, **37**, 239–245.
- HODGSON, D.A., DORAN, P.T., ROBERTS, D. & MCMINN, A. 2004. Paleolimnological studies from the Antarctic and subantarctic islands. In SMOL, J.P., PIENITZ, R. & DOUGLAS, M.S.V., eds, *Long-term environmental change in Arctic and Antarctic lakes*. Berlin: Springer, 419–474.
- HOUGHTON, J. 2001. *Climate change 2001: the scientific basis. Contribution of Working Group I to the Third Assessment Report of the Intergovernmental Panel on Climate Change*. Cambridge: Cambridge University Press, 893 pp.
- HJORT, C., INGÓLFSSON, Ó., MÖLLER, P. & LIRIO, J.M. 1997. Holocene glacial history and sea-level changes on James Ross Island, Antarctic Peninsula. *Journal of Quaternary Science*, **12**, 259–273.
- INGÓLFSSON, Ó., HJORT, C. & HUMLUM, O. 2003. Glacial and climate history of the Antarctic Peninsula since the Last Glacial Maximum. *Arctic, Antarctic, and Alpine Research*, **35**, 175–186.
- JENA, B., BAJISH, C.C., TURNER, J., RAVICHANDRAN, M., ANILKUMAR, N. & KSHITIA, S. 2022. Record low sea ice extent in the Weddell Sea, Antarctica in April/May 2019 driven by intense and explosive polar cyclones. *npj Climate and Atmospheric Science*, **5**, 19.
- JOHNSON, J.S., BENTLEY, M., ROBERTS, S.J., BINNIE, S.A. & FREEMAN, S.P.H.T. 2011. Holocene deglacial history of the northeast Antarctic Peninsula - a review and new chronological constraints. *Quaternary Science Reviews*, **30**, 3791–3802.
- KANFOUSH, S.L., HODELL, D.A., CHARLES, C.D., JANECEK, T.R. & RACK, F.R. 2002. Comparison of ice-rafted debris and physical properties in ODP Site 1094 (South Atlantic) with the Vostok ice core over the last four climatic cycles. *Palaeogeography, Palaeoclimatology, Palaeoecology*, **182**, 329–349.
- KAPLAN, M., STRELIN, J., SCHAEFER, J., PELTIER, C., MARTINI, M., FLORES, E., *et al.* 2020. Holocene glacier behavior around the northern Antarctic Peninsula and possible causes. *Earth and Planetary Science Letters*, **534**, 116077.
- KREK, A.V., KREK, E.V. & KRECHIK, V.A. 2021. The circulation and mixing zone in the Antarctic Sound in February 2020. In MOROZOV, E.G., FLINT, M.V. & SPIRIDONOV, V.A., eds, *Antarctic Peninsula region of the Southern Ocean*. Advances in Polar Ecology, vol. **6**, 83–99.
- KUMAR, A., YADAV, J. & MOHAN, R. 2021. Seasonal sea-ice variability and its trend in the Weddell Sea sector of West Antarctica. *Environmental Research Letters*, **16**, 024046.
- KWOK, R. & COMISO, J.C. 2002. Spatial patterns of variability in Antarctic surface temperature: connections to the Southern Hemisphere Annular Mode and the Southern Oscillation. *Geophysical Research Letters*, **29**, 50-51–50-54.
- LINDHORST, S. & SCHUTTER, I. 2014. Polar gravel beach-ridge systems: sedimentary architecture, genesis, and implications for climate reconstructions (South Shetland Islands/western Antarctic Peninsula). *Geomorphology*, **221**, 187–203.
- MAJEWSKI, W. & ANDERSON, J.B. 2009. Holocene foraminiferal assemblages from Firth of Tay, Antarctic Peninsula: paleoclimate implications. *Marine Micropaleontology*, **73**, 135–147.
- MARSHALL, G.J., ORR, A., VAN LIPZIG, N.P. & KING, J.C. 2006. The impact of a changing Southern Hemisphere Annular Mode on Antarctic Peninsula summer temperatures. *Journal of Climate*, **19**, 5388–5404.
- MASSON-DELMOTTE, V., STENNI, B. & JOUZEL, J. 2004. Common millennial-scale variability of Antarctic and Southern Ocean temperatures during the past 5000 years reconstructed from the EPICA Dome C ice core. *The Holocene*, **14**, 145–151.
- MICHALCHUK, B.R., ANDERSON, J.B., WELLNER, J.S., MANLEY, P.L., MAJEWSKI, W. & BOHATY, S. 2009. Holocene climate and glacial

- history of the northeastern Antarctic Peninsula: the marine sedimentary record from a long SHALDRIL core. *Quaternary Science Reviews*, **28**, 3049–3065.
- MILLIKEN, K., ANDERSON, J., WELLNER, J., BOHATY, S. & MANLEY, P. 2009. High-resolution Holocene climate record from Maxwell Bay, South Shetland Islands, Antarctica: Holocene climate record from Maxwell Bay. *Geological Society of America Bulletin*, **121**, 1711–1725.
- MORENO, P., VILANOVA, I., VILLA-MARTÍNEZ, R., DUNBAR, R., MUCCIARONE, D., KAPLAN, M., *et al.* 2018. Onset and evolution of Southern Annular Mode-like changes at centennial timescale. *Scientific Reports*, **8**, 1–9.
- MULVANEY, R., ABRAM, N.J., HINDMARSH, R.C., ARROWSMITH, C., FLEET, L., TRIEST, J., *et al.* 2012. Recent Antarctic Peninsula warming relative to Holocene climate and ice-shelf history. *Nature*, **489**, 141.
- MURRAY, A.S. & WINTLE, A.G. 2000. Luminescence dating of quartz using an improved single-aliquot regenerative-dose protocol. *Radiation Measurements*, **32**, 57–73.
- NICHOLS, R.L. 1961. Characteristics of beaches formed in polar climates. *American Journal of Science*, **259**, 694–708.
- NIE, S., XIAO, W. & WANG, R. 2022. Mid-late Holocene climate variabilities in the Bransfield Strait, Antarctic Peninsula driven by insolation and ENSO activities. *Palaeogeography, Palaeoclimatology, Palaeoecology*, **601**, 111140.
- NYVLT, D., BRAUCHER, R., ENGEL, Z., MLČOCH, B. & ASTER Team. 2014. Timing of the Northern Prince Gustav Ice Stream retreat and the deglaciation of northern James Ross Island, Antarctic Peninsula during the last glacial-interglacial transition. *Quaternary Research*, **82**, 441–449.
- ORSI, A.H., NOWLIN JR, W.D. & WHITWORTH III, T. 1993. On the circulation and stratification of the Weddell Gyre. *Deep-Sea Research I*, **40**, 169–203.
- PALACIOS, D., RUIZ-FERNÁNDEZ, J., OLIVA, M., ANDRÉS, N., FERNÁNDEZ-FERNÁNDEZ, J.M., SCHIMMELPFENNIG, I., *et al.* 2020. Timing of formation of neoglacial landforms in the South Shetland Islands (Antarctic Peninsula): regional and global implications. *Quaternary Science Reviews*, **234**, 106248.
- PARKINSON, C.K. & CAVALLERI, D.J. 2012. Antarctic sea ice variability and trends, 1979–2010. *Cryosphere*, **6**, 871–880.
- PARKINSON, C.K. & DIGIROLAMO, N.E. 2021. Sea ice extents continue to set new records: Arctic, Antarctic, and global results. *Remote Sensing of Environment*, **267**, 112753.
- POWERS, M.C. 1953. A new roundness scale for sedimentary particles. *Journal of Sedimentary Research*, **23**, 117–119.
- PRESCOTT, J.R. & HUTTON, J.T. 1994. Cosmic ray contributions to dose rates for luminescence and ESR dating: large depths and long-term time variations. *Radiation Measurements*, **23**, 497–500.
- PRESCOTT, J.R. & STEPHAN, L.G. 1982. The contribution of cosmic radiation to the environmental dose for thermoluminescence dating. *PACT*, **6**, 17–25.
- PUDSEY, C., BARKER, P. & LARTER, R. 1994. Ice sheet retreat from the Antarctic Peninsula shelf. *Continental Shelf Research*, **14**, 1647–1675.
- REYNOLDS, J.M. 1981. The distribution of mean annual temperatures in the Antarctic Peninsula. *BAS Bulletin*, No. **54**, 123–133.
- ROBERTS, S., HODGSON, D., BENTLEY, M., SANDERSON, D., MILNE, G., SMITH, J., *et al.* 2009. Holocene relative sea-level change and deglaciation on Alexander Island, Antarctic Peninsula, from elevated lake deltas. *Geomorphology*, **112**, 122–134.
- ROBERTS, S., HODGSON, D.A., STERKEN, M., WHITEHOUSE, P.L., VERLEYEN, E., VYVERMAN, W., *et al.* 2011. Geological constraints on glacio-isostatic adjustment models of relative sea-level change during deglaciation of Prince Gustav Channel, Antarctic Peninsula. *Quaternary Science Reviews*, **30**, 3603–3617.
- RUIZ-FERNÁNDEZ, J., OLIVA, M., NYVLT, D., CANNONE, N., GARCIA-HERNÁNDEZ, C., GUGLIELMIN, M., *et al.* 2019. Patterns of spatio-temporal paraglacial response in the Antarctic Peninsula region and associated ecological implications. *Earth-Science Reviews*, **192**, 379–402.
- SCHIEFFERS, A., ENGEL, M., SCHEFFERS, S., SQUIRE, P. & KELLETAT, D. 2012. Beach ridge systems - archives for Holocene coastal events? *Progress in Physical Geography*, **36**, 5–37.
- SCHWERDTFEGER, W. 1975. The effect of the Antarctic Peninsula on the temperature regime of the Weddell Sea. *Monthly Weather Review*, **103**, 45–51.
- SHEVENELL, A. & KENNETT, J.P. 2002. Antarctic Holocene climate change: a benthic foraminiferal stable isotope record from Palmer Deep. *Paleoceanography*, **17**, PAL 9-1–PAL 9-12.
- SHEVENELL, A., INGALLS, A., DOMACK, E. & KELLY, C. 2011. Holocene Southern Ocean surface temperature variability west of the Antarctic Peninsula. *Nature*, **470**, 250.
- SIEGERT, M.J., BENTLEY, M.J., ATKINSON, A., BRACEGIRDLE, T.J., CONVEY, P., DAVIES, B., *et al.* 2023. Antarctic extreme events. *Frontiers in Environmental Science*, **11**, 1229283.
- SIMKINS, L.M., SIMMS, A.R. & DEWITT, R. 2013. Relative sea-level history of Marguerite Bay, Antarctic Peninsula derived from optically stimulated luminescence-dated beach cobbles. *Quaternary Science Reviews*, **77**, 141–155.
- SIMKINS, L.M., SIMMS, A.R. & DEWITT, R. 2015. Assessing the link between coastal morphology, wave energy and sea ice throughout the Holocene from Antarctic raised beaches. *Journal of Quaternary Science*, **30**, 335–348.
- SIMKINS, L.M., DEWITT, R., SIMMS, A.R., BRIGGS, S. & SHAPIRO, R.S. 2016. Investigation of optically stimulated luminescence behavior of quartz from crystalline rock surfaces: a look forward. *Quaternary Geochronology*, **36**, 161–173.
- SIMMS, A.R., DEWITT, R., KOUREMENOS, P. & DREWRY, A.M. 2011. A new approach to reconstructing sea levels in Antarctica using optically stimulated luminescence of cobble surfaces. *Quaternary Geochronology*, **6**, 50–60.
- SIMMS, A.R., IVINS, E.R., DEWITT, R., KOUREMENOS, P. & SIMKINS, L.M. 2012. Timing of the most recent Neoglacial advance and retreat in the South Shetland Islands, Antarctic Peninsula: insights from raised beaches and Holocene uplift rates. *Quaternary Science Reviews*, **47**, 41–55.
- SIMMS, A.R., WHITEHOUSE, P., SIMKINS, L., NIELD, G., DEWITT, R. & BENTLEY, M. 2018. Late Holocene relative sea-level reconstruction near Palmer Station, northern Antarctic Peninsula may record late Holocene ice mass changes not LGM glacial isostatic adjustment. *Quaternary Science Reviews*, **199**, 49–59.
- SIMMS, A.R., BENTLEY, M.J., SIMKINS, L.M., ZURBUCHEN, J., REYNOLDS, L.C., DEWITT, R. & THOMAS, E.R. 2021. Evidence for a 'Little Ice Age' glacial advance within the Antarctic Peninsula - examples from glacially-overtun raised beaches. *Quaternary Science Reviews*, **271**, 107195.
- SMITH, J.A., HILLENBRAND, C.-D., SUBT, C., ROSENHEIM, B.E., FREDERICH, T., EHRLICH, W., *et al.* 2021. History of the Larsen C Ice Shelf reconstructed from sub-ice shelf and offshore sediments. *Geology*, **49**, 978–982.
- STAMMERJOHN, S. & SMITH, R. 1996. Spatial and temporal variability of western Antarctic Peninsula sea ice coverage. *Foundations for Ecological Research West of the Antarctic Peninsula*, **70**, 81–104.
- STERKEN, M., ROBERTS, S.J., HODGSON, D.A., VYVERMAN, W., BALBO, A.L., SABBE, K., *et al.* 2012. Holocene glacial and climate history of Prince Gustav Channel, northeastern Antarctic Peninsula. *Quaternary Science Reviews*, **31**, 93–111.
- TOTTEN, R.L., ANDERSON, J.B., FERNÁNDEZ, R. & WELLNER, J.S. 2015. Marine record of Holocene climate, ocean, and cryosphere interactions: Herbert Sound, James Ross Island, Antarctica. *Quaternary Science Reviews*, **129**, 239–259.
- TURNER, J., HOLMES, C., HARRISON, T.C., PHILLIPS, T., JENA, B., REEVES-FRANCOIS, T., *et al.* 2022. Record low Antarctic sea ice cover in February 2022. *Geophysical Research Letters*, **49**, e2022GL098904.

- VAUGHAN, D.G., MARSHALL, G.J., CONNOLLEY, W.M., PARKINSON, C., MULVANEY, R., HODGSON, D.A., *et al.* 2003. Recent rapid regional climate warming on the Antarctic Peninsula. *Climatic Change*, **60**, 243–274.
- VERNET, M., GEIBERT, W., HOPPEMA, M., BROWN, P.J., HAAS, C., HELLMER, H.H., *et al.* 2019. The Weddell Gyre, Southern Ocean: present knowledge and future challenges. *Reviews of Geophysics*, **57**, 623–708.
- WALLINGA, J., BOS, A.J.J., DORENBOS, P., MURRAY, A.S. & SCHOKKER, J. 2007. A test case for anomalous fading correction in IRSL dating. *Quaternary Geochronology*, **2**, 216–221.
- WATCHAM, E., BENTLEY, M., HODGSON, D., ROBERTS, S.J., FRETWELL, P., LLOYD, J., *et al.* 2011. A new Holocene relative sea level curve for the South Shetland Islands, Antarctica. *Quaternary Science Reviews*, **30**, 3152–3170.
- WINTLE, A.G. & MURRAY, A.S. 2006. A review of quartz optically stimulated luminescence characteristics and their relevance in single-aliquot regeneration dating protocols. *Radiation Measurements*, **41**, 369–391.
- YU, Z., BEILMAN, D.W. & LOISEL, J. 2016. Transformations of landscape and peat-forming ecosystems in response to late Holocene climate change in the western Antarctic Peninsula. *Geophysical Research Letters*, **43**, 7186–7195.
- ZAK, J., SOEGJONO, I., JANOUSEK, V. & VENERA, Z. 2012. Magnetic fabric and tectonic setting of the early to middle Jurassic felsic dykes at Pitt Point and Mount Reece, eastern Graham Land, Antarctica. *Antarctic Science*, **24**, 45–58.
- ZURBUCHEN, J. & SIMMS, A.R. 2019. Late Holocene ice-mass changes recorded in a relative sea-level record from Joinville Island, Antarctica. *Geology*, **47**, 1064–1068.